EUROPEAN ORGANIZATION FOR NUCLEAR RESEARCH

CERN LIBRARIES, GENEVA

CERN/SPSC 88-47
SPSC/P242
22 December 1988

MEASUREMENT OF THE SPIN-DEPENDENT STRUCTURE FUNCTIONS OF THE NEUTRON AND PROTON

The Spin Muon Collaboration (SMC)

NIKHEF, FOM and Free University, Amsterdam
J. Beaufays, J. Ciborowski, R.v.Dantzig, M.v.d.Heijden,
M.d.Jong, T. Ketel, G.v.Middelkoop
University of Bielefeld
G. Baum, F. Sever, M. Siebler
CERN
T.O. Niinikoski
Delft University of Technology
H. Postma
JINR, Dubna
I.A. Golutvin, I.U.T. Kiryushin, V.N. Lysakov, D. Pose,
I. Savin, G. Smirnov, N.I. Zamyatin
University of Freiburg
A. Brüll, H. Engelien, U. Landgraf, H.E. Stier
University of Houston
E. Hungerford, K. Lau, B. Mayes, R. Phelps, L. Pinsky, J. Pyrlik, R. Weinstein
University of California, Los Angeles
J. Carroll, D. Drake†, E. Gulmez, G. Igo, S. Trentalange, C. Whitten
University of Mons
P. Pilette, R. Windmolders
Northeastern University
E.v. Goeler, J. Moromisato, E. Saletan
Rice University
D.L. Adams, B.E. Bonner, J. Buchanan, J. Clement, M.D. Corcoran, J.W. Kruk,
H.E. Miettinen, G.S. Mutchler, M. Nessi, F. Nessi-Tedaldi, J.B. Roberts
Uppsala University
A. Arvidson, B. Badelek, S. Kullander, T. Lindqvist
University of Virginia
D. Day, J. Lichtenstadt, R. Lindgren, R. Marshall, J. McCarthy, B. Norum,
D. Pocanic, R. Sealock, S. Thornton
Warsaw University and Institute for Nuclear Studies
J. Nassalski, E. Rondio, L. Ropelewski, A. Sandacz
Yale University
S. Dhawan, V.W. Hughes, V. Papavassiliou, P. Schüler
ETH, Zürich*
W. Gruebler

* Tentative, †Los Alamos National Laboratory

Spokesman : V.W. Hughes
Contactman: R. Windmolders

ABSTRACT

We propose a new measurement of spin-dependent asymmetries in the deep inelastic scattering of polarized muons by polarized protons and deuterons in an experiment similar to the EMC polarization experiment, using a modified CERN/EMC polarized target, the EMC/NMC spectrometer and including a muon polarimeter. The measurement will determine the spin-dependent structure functions of the proton and neutron, $g_1^p(x)$ and $g_1^n(x)$, in the scaling regime from x = 0.01 to x = 0.7 and hence their first moments $\Gamma = \int_0^1 g_1(x)\,dx$. A test of the fundamental Bjorken polarization sum rule at about the 10% accuracy level should be achieved. Also tests of individual sum rules for the proton and neutron will be made. Measurements of these quantities will make it possible to test further nucleon models and to explore the contribution of quark spins to the nucleon spin.

Table of Contents

1. INTRODUCTION AND REVIEW OF CURRENT KNOWLEDGE

The spin-dependent structure functions of the nucleon contain the basic information about the spin composition of the proton and neutron and make possible important tests of QCD and of our models of the nucleon. These spin-dependent structure functions are independent of the exhaustively studied spin-independent structure functions. They are determined from measurements of spin-dependent asymmetries in the deep inelastic scattering of polarized electrons or muons on polarized nucleons[1].

Two major experiments have determined the spin-dependent structure function $g_1^p(x)$ of the proton. The first was an experiment with polarized electrons at SLAC[2] in the kinematic range x = 0.1 to x = 0.7, and the second was a recent experiment with polarized muons at CERN[3] in the broader kinematic range x = 0.01 to x = 0.7. The quantity measured in these experiments is $A_1(x) \equiv \frac{\sigma_{1/2} - \sigma_{3/2}}{\sigma_{1/2} + \sigma_{3/2}}$, in which $\sigma_{1/2}(\sigma_{3/2})$ is the absorption cross section for polarized virtual photons by polarized protons when the total component of angular momentum along the collision axis is 1/2 (3/2). The results of the two experiments are shown in fig. 1. The agreement is excellent in the region of overlap from x = 0.1 to x = 0.7.

A fundamental sum rule, originally derived by Bjorken[4] from current algebra but now recognised to be based on QCD in the scaling limit relates the first moments of the spin-dependent structure functions of the nucleon to the weak interaction coupling constants for neutron beta decay. It reads

$$\int_0^1 dx \left(g_1^p(x) - g_1^n(x)\right) = \frac{1}{6}\left|\frac{g_A}{g_V}\right|\left(1 - \frac{\alpha_s(Q^2)}{\pi}\right) = 0.191 \pm 0.002 \qquad (1)$$

Here

$$g_1^{p(n)}(x) = \frac{1}{2x}\frac{A_1^{p(n)}(x)\ F_2^{p(n)}(x)}{1 + R^{p(n)}(x)} \qquad (2)$$

in which $F_2(x)$ and $R(x)$ have their usual meanings[1]. The factor involving the strong coupling constant $\alpha_s = 0.27$ at $Q^2 = 10\ GeV^2$ is the correction to the zeroth order Bjorken sum rule due to perturbative QCD[5]. In the naive quark-parton model

$$g_1(x) = \frac{1}{2} \sum_i e_i^2 \left[q_i^{\uparrow}(x) - q_i^{\downarrow}(x) \right] \tag{3}$$

where i indicates the quark type with charge e_i and where $q_i^{\uparrow(\downarrow)}(x)$ is the probability that quark of type i with fractional momentum x of the nucleon has its spin parallel (antiparallel) to the nucleon spin. Hence $\frac{1}{2}\Delta q_i(x) = \frac{1}{2}[q_i^{\uparrow}(x) - q_i^{\downarrow}(x)]$ is the contribution of quark type i with momentum fraction x to the proton spin.

Auxiliary sum rules for the proton and neutron separately, which involve nucleon model-dependent assumptions - principally the validity of flavor SU(3) and that the strange quark sea is unpolarized - have been given by Ellis and Jaffe[6] (a similar result was obtained by Belyaev et al.[7]):

$$\Gamma_p = \int_0^1 dx\, g_1^p(x) = 0.189 \pm 0.005 \tag{4}$$

$$\Gamma_n = \int_0^1 dx\, g_1^n(x) = -0.002 \pm 0.005 \tag{5}$$

The above numbers contain QCD corrections as explained in ref. 3.

Thus far, experimental data are available only for the proton so that the Bjorken sum rule cannot be tested. However, the Ellis-Jaffe sum rule for the proton given in eqn. (4) can be tested. From the CERN data alone it was found[3] that

$$\int_0^1 dx\, g_1^p(x) = 0.114 \pm 0.012\ (stat.) \pm 0.026\ (syst.) \tag{6}$$

in substantial disagreement with the theoretical prediction of eqn. (4). Combination of the CERN and SLAC data[8] gave

$$\int_0^1 dx\, g_1^p(x) = 0.116 \pm 0.009 \pm 0.019 \tag{7}$$

Figure 2 shows the CERN and SLAC data on the first moment of g_1^p as a function of the lower limit x of the integral, from which the result of eqn. (7) is derived. Note that the low x region ($x < 0.1$), measured for the first time by the EMC group, was decisive in showing the violation of the Ellis-Jaffe sum rule. The combined experimental result given in eqn. (7) disagrees more strongly with the theoretical value of eqn. (4); indeed by 3.5 standard deviations when combining statistical and systematic errors in quadrature. Furthermore, assuming the Bjorken sum rule of eqn. (1) and the experimental result of eqns. (6) and (7), we conclude that Γ_n for the neutron is much more negative (-0.075 ± 0.009 (stat.) ± 0.019 (syst.)) than the value of eqn. (5) predicted by the Ellis-Jaffe sum rule.

Finally using the Bjorken polarization sum rule of eqn. (1), the experimental results of eqn. (7), and the naive quark-parton model relation of eqn. (3), it follows that the fraction of the proton spin carried by quarks is $(3 \pm 9 \pm 17)\%$, an unexpectedly small value which implies that the spin of the proton is carried by gluons and/or orbital angular momentum. Further discussion of this conclusion is given in ref. 3.

A number of theoretical papers have recently appeared discussing the observed violation of the Ellis-Jaffe sum rule and the smallness of the spin component of the proton carried by the quark spins. A wide range of viewpoints[9-24] have been advocated to resolve or understand these problems, including the following approaches:

(1) The errors involved in deducing the first moment of the structure function have been underestimated[9], specifically those arising from the uncertainty of the extrapolation to $x = 0$.

(2) In the Q^2 range of the experiments important higher twist effects linked to the Drell, Hearn, Gerasimov sum rule exist and help to resolve the problem[10].

(3) For the Skyrme model of the nucleon in the chiral limit (where $m_q = 0$) and in the leading order of the $1/N_c$ expansion, it has been shown that none of the proton spin is carried by the quark spins. When chiral symmetry and SU(3) are broken, the contribution of the quark spins to the proton spin is still small[11]. If the chiral Lagrangian is adjusted so that the gluons carry ~ 50% of the proton momentum, then most of the orbital angular momentum L_z is carried by quarks and accounts for the proton spin[12]. However, the magnitude of the first order correction in $1/N_c$ to the above results is currently unknown.

(4) Deviations from the Ellis-Jaffe sum rule may arise[13] from the Adler-Bell-Jackiw anomaly, which could cause large variations with Q^2 in the non-perturbative regime.

(5) The Adler-Bell-Jackiw anomaly induces a gluon contribution in the singlet part of the first moment of g_1. This gluon term can in principle be large at all values of Q^2 and is consistent with a large quark spin component[14]. A related paper[15] also arrives at the conclusion that the gluon contribution to the first moment of g_1 is important, although the quantitive predictions are different from those in ref. 14. Four additional papers[16-19] also ascribe an important spin-dependent gluonic component to the proton.

(6) The effect of orbital angular momentum in a relativistic constituent quark model can be sizeable[20,21].

(7) The proton spin wavefunction may be substantially affected by gluon exchange[22].

(8) Use of flavor SU(3), which leads to the Ellis-Jaffe sum rules is unjustified, but the EMC result is nevertheless unexpected [23].

(9) The experimental results from polarized deep inelastic scattering can be interpreted to provide evidence against perturbative QCD[24].

The experimental results for $g_1^p(x)$ have important implications for searches for dark matter[25,26]. Further experiments to pursue the study of spin-dependent nucleon structure functions as well as different types of experiments are suggested[27-34]. The great diversity of theoretical interpretations and new ideas demonstrates the urgent need for new experiments.

II. SCIENTIFIC MOTIVATION AND GENERAL METHOD OF EXPERIMENT

II.1 SCIENTIFIC MOTIVATION

There has always been ample justification of a general nature to measure the spin-dependent structure functions of the nucleon; indeed a proposal was made at SLAC in 1980-82 to measure the neutron asymmetry A_1^n. The recent surprising EMC results, that the Ellis-Jaffe sum rule for the proton is violated and that only a small fraction of the proton spin is carried by the quark spins, have stimulated great interest in further measurements of the nucleon spin-dependent structure functions. Most important and fundamental will be the first measurement of the neutron spin-dependent asymmetry $A_1^n(x)$, or the neutron spin-dependent structure function $g_1^n(x)$ and its first moment Γ_n. Additionally, new proton data of higher precision are highly desirable.

Measurements of the spin dependent structure functions of the proton and the neutron

- will allow a test of the fundamental Bjorken polarization sum rule eqn. (1). This sum rule is obtained from QCD without model-dependent assumptions; hence its experimental verification will be of fundamental importance.

- will provide a further basis for testing model-dependent sum rules, such as those from Ellis and Jaffe for the proton and neutron.

- will provide important new information and constraints concerning the spin-isospin structure of the nucleon.

- are essential for understanding high energy scattering processes which involve polarized nucleons[35-38]. These include hadron-hadron scattering, the polarized Drell-Yan process and production of polarized W or Z vector bosons in collisions of polarized protons in a high energy storage ring.

II.2 GENERAL METHOD

Our proposed experiment can be viewed as an extension of the recent EMC experiment[3]. A new target system will provide polarized deuterons as well as polarized protons. The asymmetry (A) for longitudinally polarized muons scattered by longitudinally polarized nucleons is defined as

$$A = \frac{d\sigma^{\uparrow\downarrow} - d\sigma^{\uparrow\uparrow}}{d\sigma^{\uparrow\downarrow} + d\sigma^{\uparrow\uparrow}} \tag{8}$$

where $d\sigma^{\uparrow\uparrow(\uparrow\downarrow)}$ is the cross section for parallel (antiparallel) muon and nucleon spins. It is derived from the measured asymmetry

$$A = A_{meas} / (P_\mu P_T f) \tag{9}$$

where P_μ and P_T are the beam muon and target polarizations and f is the dilution factor arising from unpolarized material in the target. In first order QED, the asymmetry A is related to the virtual photon - nucleon asymmetries A_1 and A_2 by

$$A = D(A_1 + \eta A_2) \tag{10}$$

where D and η are functions of the kinematical variables. To a good approximation $A_1 = A/D$.

The aim of this experiment is to measure the proton and neutron asymmetries A_1^p and A_1^n and to determine the spin dependent structure functions in order to test the Bjorken sum rule with about 10% accuracy. The neutron asymmetry will be derived from the proton and deuteron asymmetries A_1^p and A_1^d by the relation

$$A_1^n = \frac{1 + F_2^p/F_2^n}{1 - 1.5\, w_D} A_1^d - \left(F_2^p/F_2^n\right) A_1^p \tag{11}$$

where w_D represents the D-state probability of the deuteron (~ 5%). The Bjorken sum rule will be evaluated from eqns.(1) and (2)

To reduce the systematic errors on the measured asymmetries it is essential to reverse the nucleon spins frequently and thus rapidly. In this way effects due to drift in the acceptance are largely avoided. We aim to measure P_μ with an accuracy of 5% using the polarization dependence of the muon decay spectrum, and P_T to an accuracy of 3% (see chapter III for details).

III. EXPERIMENTAL APPARATUS AND METHOD

Considerable upgrading of the EMC spectrometer, including the on-line computer and data acquisition system and additional tracking chambers, has been done by the NMC which is presently using this spectrometer (experiment NA37). Further improvements and extensions are planned for the new experiment, notably for the polarized target and muon polarimeter. See figure 3 for a schematic diagram of the experimental apparatus. In the following section details and newly needed components of the experimental apparatus are discussed.

III.1 MUON POLARIZATION MEASUREMENT

The polarization of the incident muon beam will be measured from the spectrum of the decay electrons though in a different way than has been done previously[39]. The goal in precision for measuring P_μ, which is expected to be about 80%, is 5%. Monte Carlo calculations of the muon polarization will be improved. In addition we plan to develop a promising new method based on elastic muon-electron scattering from a magnetised iron target[40].

III.1.1 Introduction

In the ideal case of monochromatic pion and muon beams, the muon beam polarization can be calculated from simple kinematics. In reality, however, the beam line has finite acceptance, which is a complicated function of the pion and muon energies and emission angles. Therefore, the calculation of the polarization requires a detailed simulation of the beam line with all its magnetic elements. Such a Monte Carlo simulation[41] was used by EMC to calculate the polarization with an estimated accuracy of about 8%. This calculation was found to be in agreement with measurements performed[39] for the NA4 experiment which had an accuracy of 10-15%.

It is hoped that a study of the Monte Carlo simulation of the beam will lead to a better understanding of it, resulting in a reduced uncertainty in the calculated polarization. In addition, we propose to measure the polarization using an improved implementation of the method used in the past [39] and which is described below.

III.1.2 Method

The muon decay method is based on the forward-backward asymmetry in the positron direction with respect to the muon spin in muon decay. In the laboratory frame, the energy spectrum of the decay positrons is given by[42]

$$\frac{dN}{dy} = \frac{N'}{N_o}\left[\left(\frac{5}{3} - 3y^2 + \frac{4y^3}{3}\right) - \left(\frac{1}{3} - 3y^2 + \frac{8y^3}{3}\right) P_L\right] \qquad (12)$$

where P_L is the longitudinal muon polarization, $y = E_{e+}/E_{\mu+}$ is the fraction of the parent-muon energy carried by the positron and $N'/N_o = 1.6 \times 10^{-4}\ D(m)/P_\mu(GeV/c)$ is the total number of decays per beam muon from the decay region of length D. Figure 4 shows the shape of the spectrum for different muon polarizations. The highest sensitivity to the muon polarization is around y = 0.75 measured by the magnitude of the spectrum and at y = 0.4 or 1.0 by the slope.

The polarimeter, proposed here, is an improvement over the one used previously to measure the polarization of the same beam, described in detail in ref. 39. The previous polarimeter, consisting of a few simple scintillator and lead glass elements, was installed immediately downstream of the last 24 mrad bend of the M2 beam line. Decay positrons were deflected downwards and out of the muon beam into the polarimeter. A Monte Carlo simulation of the beam was used to calculate the expected rates as a function of y. Within their uncertainties of 10-15%, the measurements agreed with the Monte Carlo calculations.

III.1.3 Implementation

The polarimeter will be set up downstream of the experiment (fig. 5). A plug is placed in the beam hole in the final steel wall to absorb positrons from upstream muon decays. The beam is refocused by the quadrupole triplet (Q_1 - Q_3) and remaining positrons, including those generated in the absorber, are vetoed by the shower counter (SV) downstream of the quads. Thus the beginning of a controlled field free decay region is established. The muons decay over a distance of about 35 metres, while being tracked by beam proportional chambers (BC1-6) until they reach the dipole MNP26. The decay positrons are deflected to the right into a horizontal scintillator lead glass hodoscope

(H1,LG) immediately downstream of a proportional chamber system used for determination of the momentum dependent trajectory.

The lead glass is used for positron identification in the trigger and provides an energy measurement as a cross check on the momentum measurement made with the chambers. Incompatibility between the two measurements allows discrimination against positrons arising from muon decays in the magnet. Depending on the energy resolution of the lead glass counters, 90-95% of this background is eliminated, leaving only a residual background of 1-2% in the spectrum used for the polarization measurement. An optional synchroton radiation detector may serve as an additional means of rejecting background[39,43]. Most of the decay volume will be in vacuum to reduce positron interactions in air.

The spectral range that can be covered depends on the excitation of the magnet and on the minimum allowable distance of the lead glass from the beam. With the configuration shown in fig. 5 this range is approximately $0.2 < y < 0.7$. The maximum attainable y is determined by the beam diameter at the lead glass which is expected to be about 5 cm FWHM.

The muon decay in the field free region should give rise to a positron spectrum with little distortion compared to the theoretical shape shown in fig. 4. The slope of the spectrum near $y = 0.4$ is a measure of the muon polarization independent of the beam flux normalisation. The absolute magnitude of the spectrum around $y = 0.7$, normalised to the beam flux, is also a sensitive measure of the muon polarization.

The measured yields will be corrected for the acceptance of the polarimeter which, we believe, can be determined to within 3%. The relative acceptance of different y bins should be known to an even higher accuracy. The random trigger method[44] used by the EMC for monitoring the beam flux is accurate to 2%.

An important advantage of this downstream polarimeter is that the muons which decay will have been tagged by the beam momentum hodoscopes, so that the variable $y = E_{e^+}/E_{\mu^+}$ of the decay spectrum is precisely known on an event by event basis, which enhances the accuracy of the measurement.

We estimate that systematic errors (tab. 3.1) will dominate the statistical error and that an overall error of 5% can be achieved. We expect 300 useful positron/10^7 beam muons decaying into the polarimeter. For testing and setting up we expect to record more than

10^5 μ decays/hour, which gives greater statistical accuracy than the estimated systematic errors. During normal data acquisition this will be prescaled to about 10^4/hour which still gives a rapid measurement.

Table 3.1
Systematic Errors

Source	Estimated Magnitude
Beam Normalisation	2%
Beam Phase Space	2%
Spectrometer Acceptance	3%
Background	2%

The polarimeter apparatus could be supplemented with additional detectors and readout electronics that would also allow measurement of the muon polarization by elastic μ-e scattering on a magnetised iron target[40].

III.1.4 Muon Polarimeter Equipment

Four beam multiwire proportional chambers (MWPC's), similar to those now in use by the NMC, must be constructed. Lead glass shower counters, a scintillator hodoscope as well as three larger MWPC's are to be built. The magnet MNP26 and its power supply are already in use by the NMC. Three standard PS quadrupoles with power supplies must be obtained. The equipment required is shown in the following table.

Table 3.2
Equipment for Muon Polarimeter

Equipment	Quantity	Status
MNP26 Dipole + power supply	1	In use by NMC
PS Quad + power supply	3	To be procured
Beam proportional chambers	2 4	In use by NMC To be built
Shower veto counter	1	To be built
Proportional chambers	3	To be built
Trigger scintillator hodoscopes	1	To be built
Lead glass counters	6	To be built

III.2 POLARIZED PROTON AND DEUTERON TARGET

III.2.1 Introduction

Our polarized target will make use of parts from the CERN/EMC target[45,46]. The method of dynamic nuclear polarization (DNP) is used to polarize the target[47,48]. There are two new major requirements for our experiment, (1) to polarize deuterons as well as protons, and (2) frequent reversal of the target polarization. New equipment, most importantly a solenoid/dipole magnet will be needed to meet these new requirements. We aim for a new twin-target, each half being 60 cm long and 4 to 5 cm in diameter with a 30 cm spacing between the two target halves. The new polarizing magnet will be a solenoid approximately 220 cm long and 28 cm in diameter. Special new features for the polarized target and the related R&D efforts will be discussed in the following subsections.

III.2.2 Target Configuration and Target Material

The polarized target will be operated analogously to the EMC twin-target configuration (fig. 6) with its two halves having opposite polarizations. These polarizations in opposite directions are obtained simultaneously by using slightly different microwave frequencies in the two cavities of the twin-target. Leakage of microwaves between the cavities of the two halves may be more harmful for the polarization of deuterons than in the case of protons; we plan to test this before operating the target in the experiment. In the event of significant depolarization due to leakage, as compared with the almost negligible losses in the EMC polarized ammonia target, we shall improve the microwave isolation between the cavities. This requires a study of microwave absorbing materials at low temperatures, and tighter fabrication and assembly tolerances for the target cavities. This investigation will be pursued in collaboration with one of the university groups.

We propose to operate the target in the frozen-spin mode, in order to allow polarization reversal by field rotation. This requires a lower base temperature (50 mK compared with 80 mK previously), which can be reached by improving the thermal grounding inside the target holder assembly. This part must be reconstructed also for other reasons.

We plan to use as target material (deuterated) butanol mixed with about 5% of (deuterated) water to promote glass formation. The material will be prepared in the form of small beads, obtained by letting droplets freeze in direct contact with liquid nitrogen. As paramagnetic (deuterated) dopant EHBA-Cr(V), which is commercially available now, will

be used. The preparation of the material will be optimised by testing samples in the PS 199 polarized target setup at CERN.

III.2.3 Solenoid/Dipole Magnet

A new magnet is needed for two principal reasons. The first is to provide a longitudinal field of 2.5T over the target volume with high homogeneity ($\pm$ 2 x 10^{-5} rather than $\pm$ 10^{-4} for the EMC magnet), to achieve highest deuteron polarization (because of the lower spin temperature required for the deuteron).

The second reason is to provide a transverse dipole magnetic field. A dipole field of 0.1T will be used for the method of spin reversal by field rotation (see section III.2.5), while a dipole field of 0.5T allows a transverse proton polarization for an exploratory measurement of A_2^p (see section IV). The transverse dipole field need not be homogeneous because the proton polarization is maintained in the frozen spin mode.

III.2.4 Polarization Measurement

The target polarizations P_T will be derived using equation

$$P_T = \frac{S}{S_{cal}} \frac{G_{cal}}{G} P_{cal} \qquad (13)$$

where S is the integrated polarization signal after applying DNP, and S_{cal} is the calibration signal obtained with the target in thermal equilibrium without applying DNP. Further, G and G_{cal} are the gains in the electronics for these two cases of polarization. P_{cal} is the polarization of the target in thermal equilibrium according to

$$P_{cal} = \frac{h}{2\pi} \frac{\gamma BI(I+1)}{3kT} \qquad (14)$$

An important restriction for the accuracy of determining the target polarization is the error of the temperature (T) due to temperature non-uniformity over the target, the inaccuracy of the international temperature scale etc. Small errors in γ and the magnetic field (B) can be neglected. The various sources of errors related to the integrated polarization signals and gain factors amount to about 1%. The total relative error of the deuteron and proton polarization measurements, including uncertainties in the temperature measurement, will be about 3%..

For the deuteron polarization measurement a 16 MHz NMR setup will be constructed, featuring 8 channels of simultaneous parallel measurement in 8 distinct localised NMR coils. This requires two microprocessors and two interfaces in a CAMAC crate, both handling 4 channels simultaneously. These units can be obtained commercially.

The polarization reversal by adiabatic fast passage[47] will require the installation of 16 MHz resonators to both cavities. The RF field in these must cover the target volume with moderate homogeneity requirement. The resonators can also be used for overall polarization measurements in each half of the twin-target.

The deuteron target polarization measurement will be calibrated using the following independent methods:

(i) Comparison of the deuteron polarization signal with the signal obtained when the target is at thermal equilibrium with the helium bath (1 K).

(ii) Comparison of the deuteron-NMR signal with the proton-NMR signal arising from the target residual protons in dynamic thermal equilibrium with each other after DNP; this is called spin temperature calibration.

The deuteron polarization can also be obtained from the asymmetry of the deuteron-NMR line: this procedure may give about 2% accuracy assuming homogeneous target polarization within the coil volume (this requires a high homogeneity of the magnetic field) and a linear measurement circuit with a phase-sensitive RF detector.

The proton target polarization will be measured as in the previous EMC experiment where an accuracy of 4 to 5% was obtained. With our new solenoid and with improved measurement techniques we expect to achieve also an accuracy of 3% in measuring P_p.

III.2.5 Polarization Reversal

We propose to use three methods of target polarization reversal:

(a) Reversal by rotating the magnetic field.

The target polarization will be frozen at about 50 mK for this operation. The axial holding field in frozen spin operation will be 0.5 T. The reversal time is estimated to be 1/2 hour.

(b) Reversal by fully depolarizing and repolarizing the target by retuning the microwave frequency.

The reversal time is estimated to be up to 8 hours.

(c) Reversal by adiabatic fast passage, followed by DNP.

We will study the possibility of reversing the sign of the target spin polarization by adiabatic fast passage with magnetic field sweeping followed by microwave DNP with computer optimisation. We believe that it is possible to reach at least 98% of the dynamic equilibrium value of the deuteron polarization. The reversal time may be of order 10 min.

The fast adiabatic reversal technique consists of sweeping the magnetic field through resonance while applying a relatively strong transverse RF field in the target volume. In small samples this technique achieves over 80% adiabatic efficiency. Completing the last 20% by DNP will take much less time now, compared with reversal by normal DNP, case (b). Strong evidence of this is in the observation that zeroing the target polarization, before reversal by DNP, will already substantially speed up the achievement of the last 20% of the polarization. This effect can be explained by slow spin diffusion in the target material, and can be verified (as is often done) by turning microwaves off for a few minutes during DNP; turning the microwaves back on results in a fast growth of the polarization until the curve limited by spin diffusion is reached.

We propose to reverse the spin and field direction once every 8 hours by method (a) and once every several days by (b). If method (c) is successful, more frequent reversals will be made.

III.2.6 Target Components

The proposed target is based on several components of the EMC polarized proton target. The following items are available.

- Dilution refrigerator;
- Target holder (this requires new coaxial lines and target support structure);
- ^{3}He pumps and gas handling system;
- ^{3}He charge of 730 litre atm (200 litre atm needs to be added);
- Microwave components and HV supplies for operation at 70 GHz;
- NMR interface for fast polarization measurement (one 4-channel unit available, a second one and a spare unit must be constructed);

- CAMAC processor and software for driving the NMR interface (a second one and a spare must be purchased).

It is assumed that CERN would provide the installation of a cold box, helium transfer line and 1700 litre dewar which were used in the EMC experiment.

III.2.7 Test Program, Installation and Time Scale

Tests of materials, deuteron polarization and the adiabatic fast passage technique will be made with the existing CERN PS 199 polarized target. The major construction item is the superconducting solenoid. It will determine the time scale for realisation of the target. The design work for this item has already started in order to meet our goal of being ready to run in 2 years.

III.2.8 Options

- A 5 Tesla field capability instead of 2.5 Tesla. This may allow us to achieve a significantly higher deuteron polarization. There would be additional costs, however, for a 140 GHz microwave system and a different NMR system, which will be necessary to implement this option.

- The possibility of employing a very interesting new polarized target material, irradiated ^{6}LiD and ^{7}LiH, which is under investigation at Saclay and which offers considerably higher effective target polarizations.

Table 3.3
Operating Conditions for Polarized Target

Target Material	Butanol and deuterated butanol (Doped with EHBA-Cr(V))
Magnet Field	2.5T
Temperature	0.5 K for DNP mode 0.05 K for frozen spin mode
Polarization	0.8 for proton; 3% rel. error 0.4 for deuteron; 3% rel. error

III.3 BEAM AND SPECTROMETER

III.3.1 Introduction

The determination of spin asymmetries in deep inelastic muon-scattering is essentially a measurement of inclusive cross section ratios. The main requirements for the spectrometer are therefore the unambiguous reconstruction of the muon vertex and its kinematic variables x and Q^2 with high efficiency and time stability.

Through the utilisation of a twin-target with its two halves polarized in opposite directions and exposed to the muon-beam at the same time, together with a regular spin-reversal the systematic effects due to flux normalisation and acceptance errors are eliminated.

The stability of all spectrometer components (beam definition, momentum measurement and tracking components) together with the stability of the beam parameters (emittance, position, time structure and polarization) is more important than the exact knowledge of the value of the acceptance which would be vital for absolute structure function measurements. Special attention is required to guarantee the unambiguous assignment of an event to either of the target halves. The longitudinal vertex resolution which is needed depends on the kinematical region (x,Q^2) and will limit the kinematical range towards small scattered angles and low muon momentum at a given separation of two targets.

III.3.2 Description of the Spectrometer

The spectrometer for the proposed experiment will be based on the EMC muon spectrometer[49] which is presently used by NMC (fig. 3). A few modifications are proposed to improve the efficiency and stability of the beam and the detection of the scattered muon.

III.3.3 Beam Definition

The beam momentum is determined in the Beam Momentum Station (BMS), a 24 mrad vertical down bend together with two hodoscopes with horizontal strips in front of and behind the bend. Reconstruction of beam tracks is possible with 3 coincident hits in the 4 BMS planes. Past experience has shown that by failure of a few central elements efficiency losses of up to 15% can occur. An increased redundancy by the addition of two

hodoscope planes is therefore proposed. This will also improve the reconstruction efficiency at high instantaneous beam intensity of 2×10^7 sec^{-1} as they are envisaged for the new experiment. The present installations would allow for such an extension.

The existing M2 muon beam has been designed for a maximum energy of 280 GeV and for use with two experiments (NA2 and NA4). Discussions with those responsible for the M2 beam in the SPS division have led to plans for a reoptimisation of the beam line for a muon energy of 100 GeV and for the presently proposed experiment; these plans involve only a rearrangement of the existing beam elements. The goal should be to obtain a reduced beam halo, a better momentum determination of the beam muons and reduction of the beam to a diameter of less than 4.5 cm.

The beam hodoscopes were rebuilt in 1986; they perform satisfactorily. An improvement of the time resolution of the large veto wall is envisaged to reduce the random veto effects which could suppress up to 20% of the scattering events at the high beam intensities projected.

III.3.4 Scattered Muon Measurement

The momentum determination of the scattered muons is based on a 1×2 m^2 window dipole magnet. The magnetic field has been mapped previously. We propose the installation of an NMR probe to improve the reproducibility of the field setting.

The wire chambers in the magnet ($3 \times (z,y,\theta)$) have been recently refurbished with new sense wire planes. A spare chamber has to be completed. Improvements of the cooling system for the preamplifiers located inside the spectrometer magnet and a revision of the low voltage power distribution are planned.

The PØ chambers covering the small angle region and the dead areas of the large chambers will be exposed to high beam currents. To be able to supply the corresponding electrical current we would like to increase the number of HV-power supplies to feed each of their 8 planes separately.

The drift chambers W12 behind the magnet are a mix of chambers with one and three potential wires. The drift chambers with 3 potential wires have lower nonlinearities and higher efficiency near the potential wires. However, they suffer from a larger sensitivity to mechanical distortions. We plan to redesign the wire positioning and fastening system in

order to better control the mechanical tolerances inside the chamber. All planes will be equipped with 3 potential wires per drift cell. The new design is currently being evaluated in a test setup in Freiburg.

The W45 system of drift chambers, located in front of the hadron absorber, has cells with a 2 cm drift space and one potential wire. It was refurbished in 1986 and the problem of dramatic aging (which was still there during the EMC polarized target runs) was eliminated. The flux of particles through this chamber is, however, rather high (mainly from electromagnetic showers) and so the reconstruction efficiency decreases with increasing beam intensity, especially on the 64 wire z-planes. For the same reason the number of planes in the W45 system for track reconstruction is just enough. Spare planes do not exist.

It is therefore planned to upgrade and improve the W45 system, consisting now of 4 chambers, by building two new chambers. The wire spacing in the new chambers will be reduced to 1 cm, at least in the central part. Two of the old chambers could then serve as spares or could stay in the experiment to improve redundancy. The additional electronics needed for the new chambers should be based on the same drift time measurement and encoder system as is used for the rest of the drift chambers in the experiment. It could come partly from the dismantled W67B system and partly from other experiments that have been phased out at CERN. For our use the performance of such a system is appropriate. The question of maintenance has to be arranged with the EP electronics division. Preamplifiers suited for the smaller wire spacing have to be obtained or reproduced.

The main problem of the current spectrometer setup is the drift chamber system W67 behind the hadron absorber. This large system of 3 sets of chambers (A,B,C in fig. 3) has a 6 cm graded field drift space. It is built from copper clad epoxy material. The material fatigue in this system (radiation and chemical aging) leads to instabilities (discharges, oscillations) which are difficult to keep under control.

We intend to replace the central (B) chambers of the W67 system, which covers the region of interest for deep inelastic muon scattering, by a streamer tube setup. The A- and C- chambers can stay in place. Since multiple scattering limits the precision with which the muon can be traced from the upstream chambers through the hadron absorber to about 1.1 cm and 6 mrad, the requirements for the spatial resolution of the muon chambers are moderate and can be met by a relatively cheap streamer tube arrangement.

III.3.5 Streamer Tube Array to Replace W67

The new detectors will consist of 16 panels of Iarocci type streamer tubes[50]. The necessary 6400 tubes could be produced in the streamer chamber assembly and research facility (SCARF) in Houston (Texas), set up by the University of Houston together with Northeastern University. The estimated failure rate for 6400 tubes altogether would be about 8 tubes per year of running and the replacement of a failed tube could be done in a short time without touching the rest of the system.

Each of the 16 panels will be read out with external 1 cm pick-up strips on either side, yielding a total of 32 coordinate measurements per track. The panels will be divided into 4 sets of 4 panels (8 coordinates) each, as shown in fig. 7a. They will be 4 x 4 m^2 in dimension and contain virtually all of the interesting events as mentioned previously. Figure 7b depicts a cross section of one set of 4 panels. A scheme of stacking is shown that will limit inefficiencies due to the intercellular walls to at most one panel per set.

To evaluate the effect of such inefficiencies and of the limited spatial accuracy on the pattern recognition and track matching routines, several Monte Carlo calculations were done. First, tracks were generated in the proposed W67B streamer tube configuration, digitising the hits and comparing the refitted line with the generated one. It was observed that the spatial error at the rear surface of the absorber, where the match with the track measured upstream is done, is about ± 2.2 mm and the error in the slope projections is 0.7 mrad. Both values are an order of magnitude less than those expected from multiple scattering in the absorber. This was confirmed by another simulation where actual data from NMC were taken. The known muon tracks in the W45 chambers were projected through the proposed streamer tubes and their response was simulated. The quality of the resulting match from lines reconstructed in the proposed W67B system and in the existing one was indistinguishable, again because of the dominance of multiple scattering. We conclude that the resolution of fitted tracks with the proposed detectors, including their inefficiencies, is more than adequate.

To further simulate the suitability of the proposed streamer tube detectors, a calculation was done to estimate from geometric considerations the anticipated efficiency for reconstructing tracks with missing coordinates. Based on experience with data from the present spectrometer, we expect this efficiency to be > 99%. Since the streamer tubes are expected to have only about 10% of the out-of-time background as compared to the present W67 chambers, the new detector system should certainly match the efficiency of the present system for those events now reconstructed. Further we anticipate that with double the

number of coordinates as compared to the present system, with the availability of a 4th projection axis, and with the lower background, some fraction of the existing events that cannot now be resolved by the pattern recognition program will be recovered with the new chamber. This can be coupled with the ability of the individual streamer tubes to run at rates in excess of 1 MHz per wire (1 cm cell) allowing the chambers to be sensitive very close to the beam. The net effect should be a considerable improvement over the present chambers in overall performance.

To read out these new streamer tubes it is proposed to use a system that is essentially commercially available. The system consists of 32 channel front-end amplifier/ discriminator/shift register cards similar to those made in the past by LeCroy, which are now fabricated by SGS. The cards of a single panel (ca. 800 channels) are daisy-chained and serviced by a single line-driver card that also supplies thresholds, low voltages, shift clocks and impedance matching. The whole system would be read out by just four CAMAC modules.

Our Dubna collaborators also propose to provide a streamer tube array to replace W67B.

III.3.6 Trigger Electronics and Data Acquisition

After a recent upgrade of the combined Romulus-Fastbus event building system, which now includes five, 1 Mbyte buffers, typically 800 events/spill can be accepted with a dead time of ~ 25%. This is sufficient to run the experiment at a flux of 4×10^7 μ/pulse. The trigger system selects muons emerging from the target region with scattering angles and momenta larger than a minimum value in order to suppress the kinematic region dominated by radiative events.

For our proposed experiment it is envisaged that the on-line data evaluation and monitoring, which have greatly improved recently using three μVAX III systems, can be advanced further by immediate track reconstruction of an adequate sample of the recorded events. This is of importance to control the possible systematic errors within the tightest possible constraints. The polarized target control and the beam polarization measurements need additional on-line systems and software.

III.3.7 Data Processing

A significant fraction of the data processing will be done on large main frame (mostly IBM and VAX) computers, partly in home institutes and partly at CERN. We expect for data-quality monitoring, first data evaluation and testing a need of typically 3000 hours (IBM168 equivalent) per year from the CERN central computing facilities during 1991-1993. For software development and simulations we need 1000 hours 168 IBM units during 1989-1990.

Production of data summary tapes will be done with dedicated multiprocessor systems. Each physics trigger requires typically one (IBM168) second of computing time. The NMC operates nine emulators (370E). Presently a prototype study is underway at NIKHEF to make use of commercially available microprocessors (e.g. 80386) each being able to run independently the reconstruction program. The system will de designed for an easy adaption of new hardware generations.

The analysis software will be basically the same as for the NMC experiment. Several modifications and extensions in the reconstruction programs due to use of new equipment and new standard software will be required.

III.3.8 Comparison with EMC Running Conditions

Because of the upgrade of the apparatus by NMC, which has resulted in improved stability and reliability, the overall loss of beam time due to detector problems (for NMC 20%) has decreased by about a factor of two since the EMC polarized target experiment. Furthermore, the beam flux that can be handled by the new data acquisition system has increased substantially. Table 3.4 presents a summary of the modifications to the apparatus since the EMC polarized target measurement, which either have already been made by NMC or are planned for the new experiment.

Table 3.4

Changes with Respect to the EMC Polarized Target Experiment

Equipment		Change	Made by	To be made by
Beam line		reoptimisation		CERN
Beam momentum stat. (BMS)	2 planes	to be constructed		CERN
Beam hodoscopes (BHA/B)	8 planes	rebuilt	NMC	
Beam polarimeter	30 planes			SMC
Beam calibr. syst. (BCS)			NMC	
Prop. chamber PV1	4 planes	new	NMC	
Prop. chamber P1,2,3	9 planes	new sense wire planes	NMC	
Prop. chamber PØ	10 planes	new	NMC	
Prop. chamber P45	2 planes	new in add. to 8 planes	NMC	
Drift chamber W45	16 planes	new sense wires	NMC	
Drift chamber W45	8 planes	to be constructed		SMC
Drift tubes W67B	16 planes	to be constructed		SMC
Small angle hodoscope	3 planes	new	NMC	
Readout	5 branches	fully spill buffered	NMC	
On-line system	3 μVAX	new	NMC	

IV. RUNNING CONDITIONS AND EXPECTED ACCURACY OF DATA

The systematic errors arising from the uncertainties in the beam and target polarizations and from various other sources listed in table 4.1 amount to 10 and 13% for the first moments of the proton and neutron structure functions, respectively, and to 10% for the Bjorken sum rule. Therefore we aim for a statistical accuracy of the order of 10% which can only be achieved within a reasonable running time at relatively low energy (E_μ = 100 GeV). The average values of Q^2 in each x interval and the expected numbers of events to be obtained in 220 days are listed in table 4.2.

A compromise between error optimisation for the neutron asymmetry and for the Bjorken sum rule leads to a division of the beam flux in the ratio 2/1 between the deuterium and hydrogen targets. The resulting running conditions and the expected statistical errors are summarised in table 4.3. The quoted values for ΔA_1^n take into account the D-state probability of the deuteron[51,52].

Table 4.1
Expected Systematic Errors

		Γ_p	Γ_d	Γ_n	Γ_p-Γ_n
Assumed Values		0.116	0.041	-0.075	0.191
Source	Estimate				
P_μ	5%	0.006	0.002	0.006	0.012
PTarget	3%	0.003	0.001	0.003	0.006
Smearing, dilution	.6%	0.001	0.000	0.001	0.002
R_{QCD}	.9%	0.001	0.000	0.001	0.002
Rad.Corr.	1.3%	0.002	0.001	0.002	0.003
F_2	5%	0.006	0.002	0.006	0.010
Neglect of A_2	$\leq\sqrt{R_{QCD}}$	0.003	0.006	0.003	0.006
Total		0.010	0.007	0.010	0.018
Percentage		10%	17%	13%	10%

With the transverse field provided by the new polarized target magnet, it will be possible to rotate the target polarization to a direction perpendicular to the beam. This configuration provides an opportunity to measure the second spin asymmetry A_2 which only gives a small contribution to the measured asymmetry when target and beam polarizations are parallel. We plan to devote a small fraction of the running time to an exploratory measurement of the A_2 asymmetry. A run of about 14 days could provide values of A_2 at low x with statistical errors smaller by a factor of 3-4 than the positivity upper limit $A_2 < \sqrt{R}$ and yield the first experimental values of $g_2(x)$ for the proton.

Table 4.2

x Interval	$\langle Q^2 \rangle$ [GeV^2]	Expected Nr. of events (in 10^6)
0.01 - 0.02	2.3	1.42
0.02 - 0.03	3.0	1.78
0.03 - 0.04	4.0	1.59
0.04 - 0.06	5.3	2.68
0.06 - 0.10	6.9	3.74
0.10 - 0.15	8.6	2.89
0.15 - 0.20	10.1	1.60
0.20 - 0.30	12.0	1.67
0.30 - 0.40	15.0	0.64
0.40 - 0.70	19.7	0.64

Table 4.3

Running Conditions and Statistical Errors

Running Time	220 Days
E_μ	100 GeV
Kinematical Range	$0.01 < x < 0.7$ $y < 0.85$ $1.5 < Q^2 < 70\ GeV^2$
Normal Flux Integrated Flux Reconstructible Flux	4×10^7 μ/pulse 63×10^{12} μ 22×10^{12} μ (Efficiency ≈ 0.35)
Beam Polarization	$(80 \pm 4)\%$
Events / μ Events, total Nr.	0.9×10^{-6} 19×10^6
Polarized Targets	Butanol $P_p = (80 \pm 2.4)\%$ 1/3 of flux Deuterated butanol $P_d = (40 \pm 1.2)\%$ 2/3 of flux
Statistical Errors	
ΔA_1^p low x	0.018 (x = 0.015)
ΔA_1^p high x	0.087 (x = 0.55)
ΔA_1^n low x	0.037 (x = 0.015)
ΔA_1^n high x	0.314 (x = 0.55)
$\Delta \int_0^1 g_1^p dx$	0.006 (~ 1/2 of EMC statistical error)
$\Delta \int_0^1 g_1^d dx$	0.009
$\Delta \int_0^1 g_1^n dx$	0.011
$\Delta \int \left(g_1^p - g_1^n\right) dx$	0.015

V. REQUIRED RESOURCES AND TIME SCALE

V.1 CAPITAL EQUIPMENT COSTS

The principal R&D tasks fall into three categories:

1. Polarized proton and deuteron target
2. Spectrometer
3. Muon Polarimeter

1. Polarized Proton and Deuteron Target (SMC, CERN)

	Estimated Costs (KSF)	
New superconducting solenoid/dipole magnet	700	SMC
Cryogenic control system with interlocks, alarms and data logging	70	CERN
Control room installation and cabling	70	CERN
Maintenance of pumps and gas handling and purifier system	90	CERN
^{3}He (200 litre-atm)	60	SMC
Target holder repair and upgrade	50	CERN
R-F Q-metres for deuteron polarization measurement	70	SMC
Purchase and preparation of deuterated materials for the target	100	SMC
Minicomputer for target operation	50	SMC
Fast reversal system, with field rotation and adiabatic fast passage	240	CERN
Total:	1500	

2. Spectrometer (SMC, CERN)

2a)	Improvement of muon beam momentum station (CERN,SPS) (two additional hodoscope planes with readout)	?	CERN
2b)	W1/2 upgrade	200	SMC
2c)	W4/5 (two new chambers with finer granularity)	600	SMC
2d)	New W67 (B-chambers) (four streamer tube chambers + readout)	800	SMC
2e)	Data acquisition and processing	200	SMC

3. Muon Polarimeter

3a)	MWPC's, counters, plus readout	600	SMC
3b)	Additional readout to allow for μ-e scattering polarization measurement	-	(option)
	Total estimated costs:	3900	KSF

V.2 ANNUAL OPERATING COSTS

SMC	(KSF)
Computer maintenance (Includes about 125KSF for maintenance of 3 microvax computers used for off-line analyses)	200
Tapes (6000 data tapes + copies with reuse) 25 SFR/Tape	150
Gases, Stores, installations, miscellaneous	130
Personnel (Secretary, collaboration members including full-time electronics engineer)	120
	600
CERN Contribution (from below)	-100
	500

CERN

EF Division:	1 technician (spectrometer) Support for polarized target maintenance and operation
EP Division:	1 data aide Travel, subsistence, general assistance on operating costs 200 KSF (including 100 KSF to be used to reduce SMC costs above)
Equipment pool:	Cover SMC costs
Central computing facilities:	1000 - 3000 (IBM168 equiv.) hours

V.3 TIME SCALE AND BEAM TIME REQUEST

We estimate that the R&D for this experiment will require 2 years and hence we hope to be ready for checkout and data-taking by early 1991. We will probably request some modest beam time in 1990 for tests of new equipment.

For the experiment we request 220 days of beam time starting 1991. One month interruption is needed to change the target material from polarized deuterium to polarized hydrogen.

REFERENCES

1. V.W. Hughes and J. Kuti, Ann. Rev. Nucl. Part. Sci. 33, 611 (1983).
2. M.J. Alguard et al., Phys. Rev. Lett. 37, 1261 (1976); 41, 70 (1978); G. Baum et al., Phys. Rev. Lett. 51, 1135 (1983).
3. EMC, J. Ashman et al., Phys. Lett. B206, 364 (1988).
4. J.D. Bjorken, Phys. Rev. 148, 1467 (1966); Phys Rev. D1, 1376 (1970).
5. J. Kodaira, Nucl. Phys. B165, 129 (1980).
6. J. Ellis and R. Jaffe, Phys. Rev. D9, 1444 (1974).
7. V.M. Belyaev, B.L. Ioffe and Ya.I. Kogan, Phys. Lett. 151B, 290 (1985).
8. V.W. Hughes et al., Phys. Lett. B212, 511 (1988).
9. F.E. Close and R.G. Roberts, Phys. Rev. Lett. 60, 1471 (1988).
10. M. Anselmino, B.L. Ioffe and E. Leader, NSF-ITP-88-94, "On Possible Resolutions of the Spin Crisis in the Parton Model".
11. S.J. Brodsky, J. Ellis and M. Karliner, Phys. Lett. B206, 309 (1988).
12. J. Ellis and M. Karliner, Phys. Lett. B213, 73 (1988).
13. R.L. Jaffe, Phys. Lett. 193B, 101 (1987).
14. G. Altarelli and G.G. Ross, Phys. Lett. B212, 391 (1988).
15. A.V. Efremov and O.V. Teryaev, JINR E2-88-287, "Spin Structure of the Nucleon and Triangle Anomaly".
16. R.D. Carlitz, J.C. Collins and A.H. Mueller, Phys. Lett. B214, 229 (1988)
17. H. Fritzsch, "The Internal Spin Structure of the Nucleon", Max-Planck-Inst. (1988)
18. E. Leader and M. Anselmino,"Understanding the Polarized EMC Experiment: The End of the Parton Spin Crisis", 1988.
19. M.Glück and E. Reya, DO-TH 88/22, "Polarized Leptoproduction and Dynamically Generated Spin Dependent Parton Distribution".
20. Z. Dziembowski, H.J. Weber, L. Mankiewicz and A. Szczepaniak, "Quark Spin and Momentum Distributions of the Nucleon", 1988.
21. G. Clément and J. Stern, "Gluons and the Spin of the Proton", CERN-TH-5216, 1988.
22. F. Myhrer and A.W. Thomas, Phys. Rev. D38, 1633 (1988).
23. H.J. Lipkin, Phys. Lett. B214, 429 (1988).
24. G. Preparata, J. Soffer, Phys. Rev. Lett. 61, 1167 (1988); A. Giannelli et al., Phys. Lett. 150B, 214 (1985).
25. J. Ellis, R.A. Flores and S. Ritz, Phys. Lett. 198B, 393 (1987).
26. J. Ellis and R.A. Flores, CERN-TH-4911/87, "Realistic Predictions for the Detection of Supersymmetric Dark Matter".

27. D.B. Kaplan and A. Manohar, Nucl. Phys. B310, 527 (1988).

28. P. Hoodbhoy, R.L. Jaffe and A. Manohar, CTP#1608, "Novel Effects in Deep Inelastic Scattering from Spin One Hadrons".

29. J.Ph.Guillet, Z. Phys. C39, 75 (1988).

30. M.C. Meng, J.C. Pan, Q.B. Xie and W. Zhu, FUB-HEP/88-9, "Origin of Proton Spin: Rotating Constituents?"

31. M. Glück and E. Reya, Z. Phys. C39, 569 (1988).

32. J. Ellis, E. Gabathuler and M. Karliner, CERN-TH-5180/88, "The OZI Rule Does Not Apply to Baryons".

33. G.P. Ramsey, J.W. Qiu, D. Richards and D. Sivers, ANL-HEP-PR-88-16, "Orbital Angular Momentum, Spin Fractions and Scenarios for the Proton's Spin-Weighted Parton Distributions".

34. G.P. Ramsey and D. Sivers, ANL-HEP-CP-88-63, "A Possible Early Experimental Test for a Large $\Delta G(x,Q^2)$".

35. F. Baldracchini et al., Int. Cent. for Theor. Phys., TrieseTech. Rep. (1980).

36. K. Hidaka et al., Phys. Rev. D21, 1316 (1980).

37. N. Craigie et al., Phys. Lett. B96, 381 (1980).

38. D. Sivers, High Energy Physics with Polarized Beams and Polarized Targets, ed. G.H. Thomas, AIP Conf. Proc. No. 51 (1978), p.505; G.P. Ramsey, D.Richards and D. Sivers, Phys. Rev. D37, 3140 (1988).

39. D. Bollini et al., Il Nuovo Cimento 63A, 441 (1981).

40. K.P. Schüler, Minneapolis Spin Conference 1988, to be published.

41. C. Iselin, "HALO, A Computer Program to Calculate Muon Halo", CERN Yellow Report 74-17 (1974).

42. S.V. Golovkin et al., Nucl. Instr. and Meth. 138, 235 (1976).

43. F.J.M. Farley, E. Picasso and L. Bracci, Nucl. Instr. and Meth. 103, 325 (1972).

44. R.P. Mount, Nucl. Instr. and Meth. 160, 23 (1979).

45. S.C. Brown et al., Proc. of 4th Int. Workshop on Polarized Target Materials and Techniques, Bonn, ed. W. Meyer (1984), p.102.

46. T.O. Niinikoski, Nucl. Instr. and Meth. 192, 151 (1982).

47. A. Abragam, "The Principles of Nuclear Magnetism", (Clarendon Press, Oxford, 1961)

48. C.D. Jeffries, "Dynamic Nuclear Orientation", (Interscience Publishers, New York, 1963).

49. EMC, O.C. Allkofer et al., Nucl. Instr. and Meth. 179, 445 (1981).

50. E. Iarocci, Nucl. Instr. and Meth. 217, 30 (1983).

51. E.L. Lomon, Ann. Phys. 125, 309 (1980).

52. T.E.O. Ericson and M. Rosa-Clot, Ann. Rev. Nucl. Part. Sci. 35, 271 (1985)

FIGURE CAPTIONS

1. Compilation[8] of all the data on A_1^p as a function of x. The EMC points and the SLAC data points (E80 and E130) are shown. Inner error bars are the statistical errors and the outer error bars are the total errors (statistical plus systematic added in quadrature). The systematic errors include uncertainties in the values of R and A_2.

2. Compilation[8] of results for $\int g_1(x)dx$. Full circles: computed from the EMC data. Open triangles: computed from the SLAC data. The solid curve was computed from a fit to the EMC data. Inner (outer) error bars are the statistical (total) errors.

3. Experimental Apparatus.

4. Decay positron energy spectra $\left(\mu^+ \rightarrow e^+ \nu_e \bar{\nu}_\mu\right)$ for different values of the muon longitudinal polarization. $y = E_{e^+}/E_{\mu^+}$.

5. Muon polarimeter.

6. EMC polarized target.

7. a) Proposed W67B streamer tube configuration (4 sets of 4 panels).
   b) Cross section of one set of 4 panels.

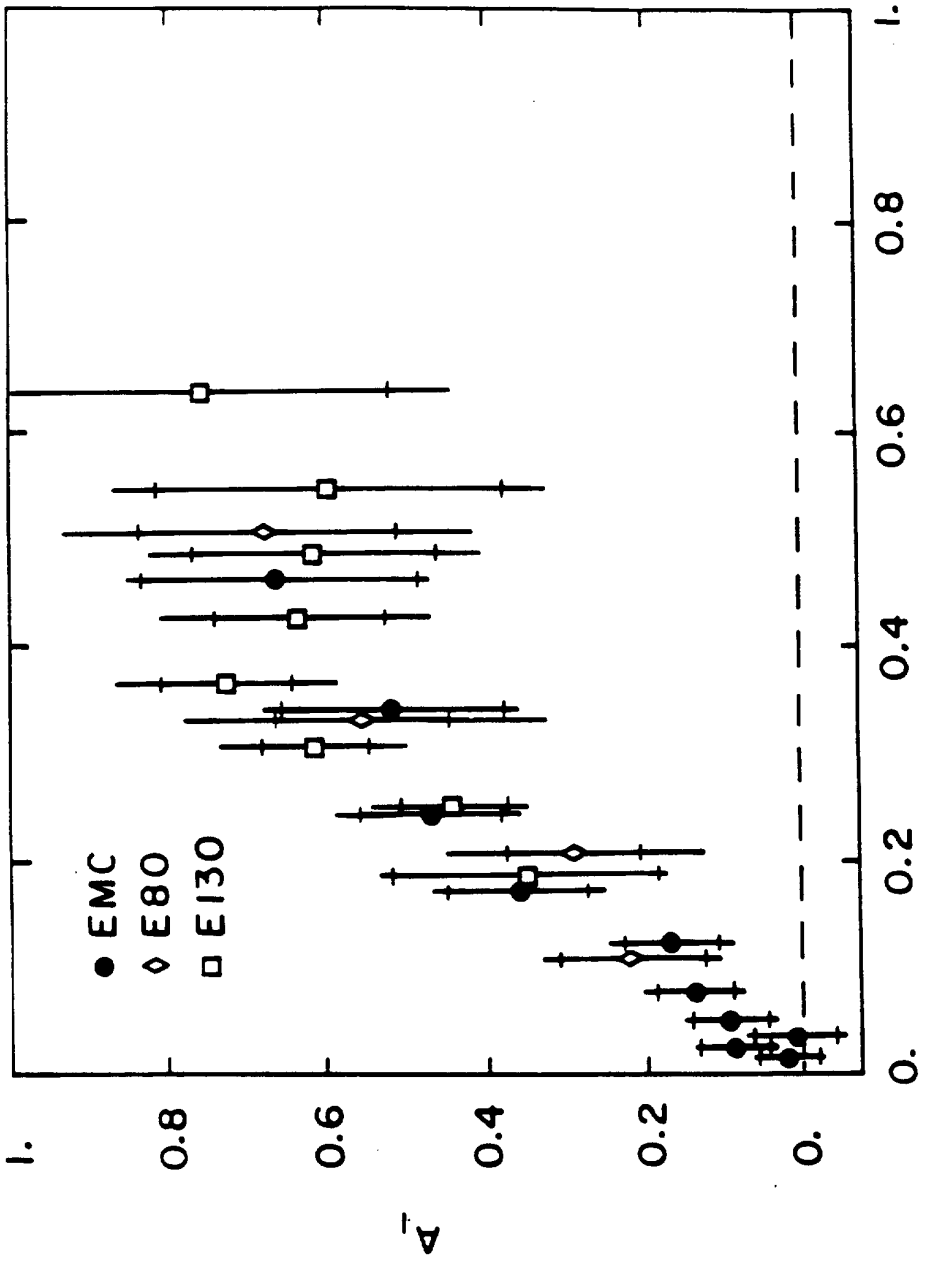

FIG. 1

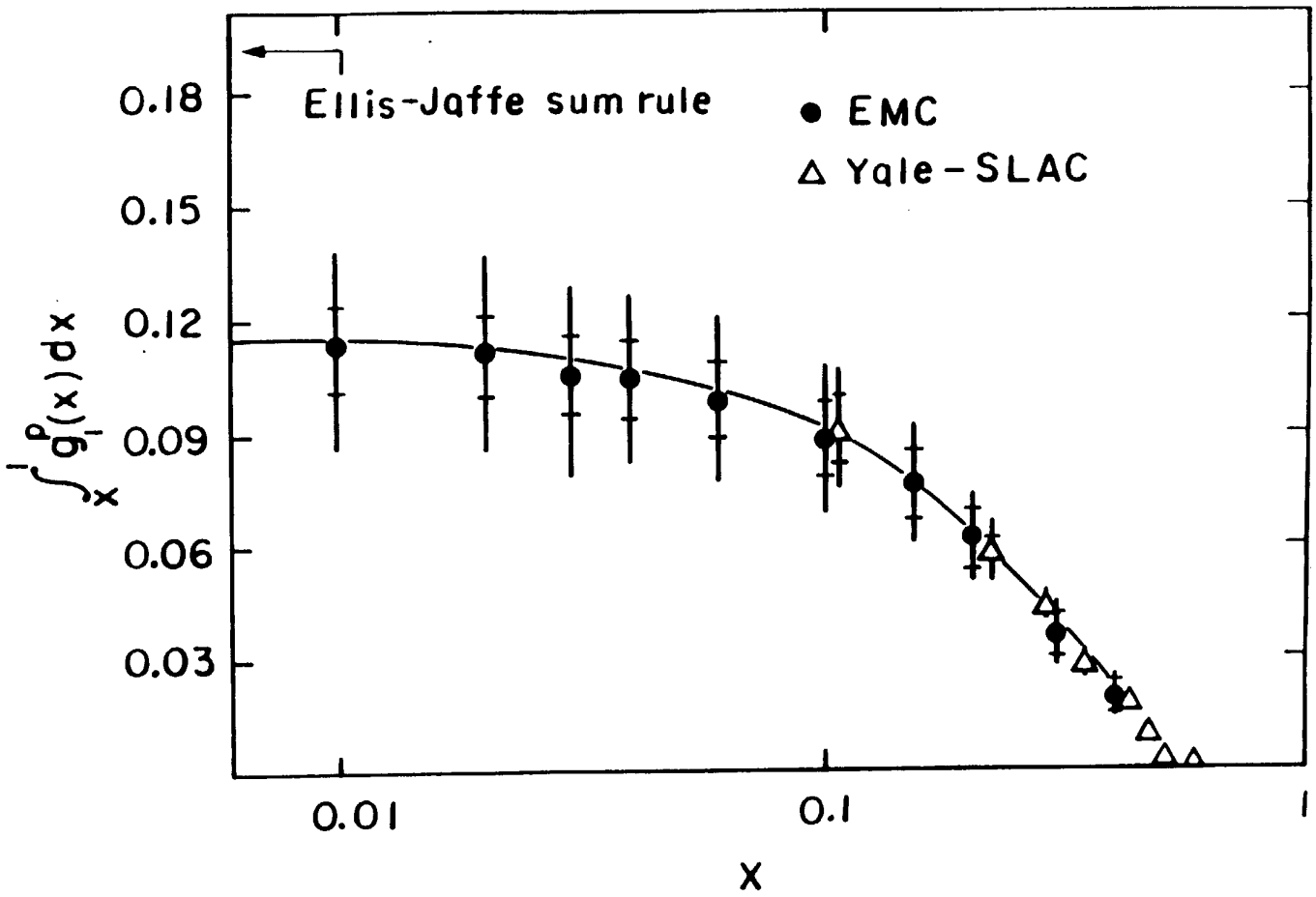
Ellis-Jaffe sum rule
EMC
Yale-SLAC
0.18
0.15
0.12
0.09
0.06
0.03
$-\int_x^1 g_1^p(x)\,dx$
0.01
0.1
1
X

FIG. 2

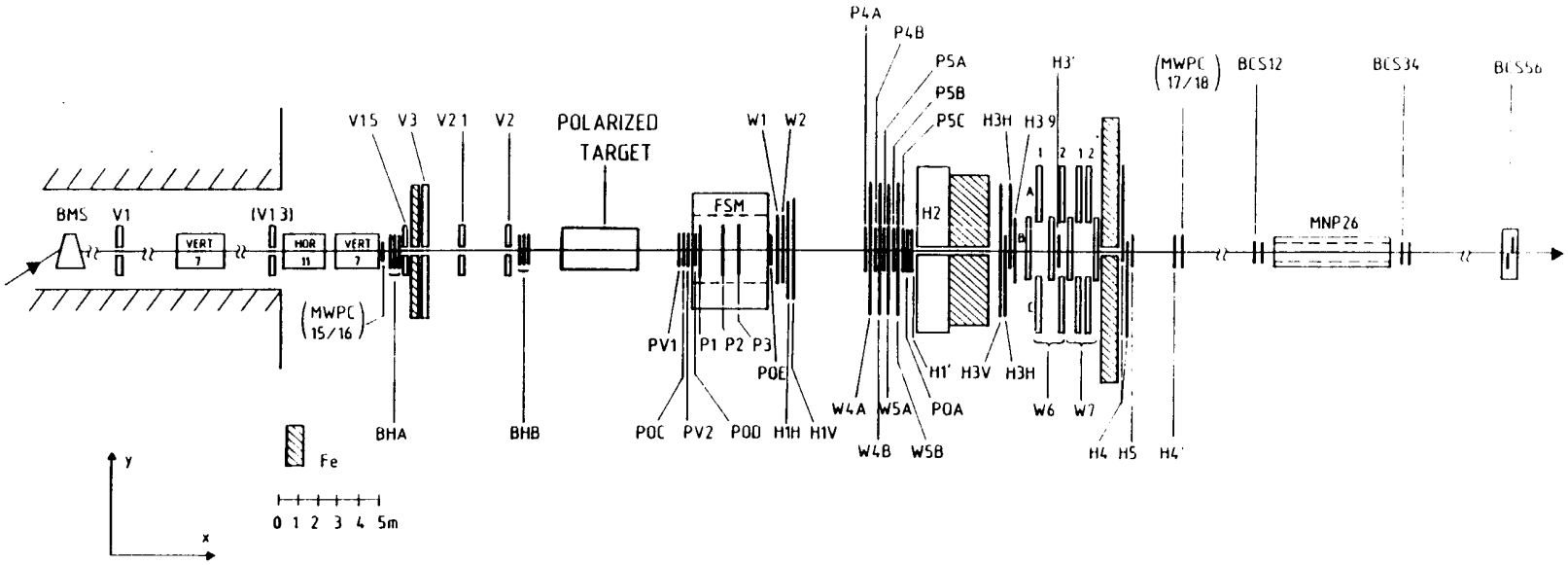
BMS
V1
VERT 7
(V13)
HOR 11
VERT 7
(MWPC 15/16)
V15
V3
V21
V2
BHA
BHB
POLARIZED TARGET
FSM
W1
W2
PV1
P1
P2
P3
POE
POC
PV2
POD
H1H
H1V
P4A
P4B
P5A
P5B
P5C
H2
W4A
W4B
W5A
W5B
POA
H1'
H3V
H3H
H3'
H3H
H3 9
W6
W7
H4
H5
H4'
(MWPC 17/18)
BCS12
BCS34
BCS56
MNP26
Fe
0 1 2 3 4 5m
y
x

FIG. 3

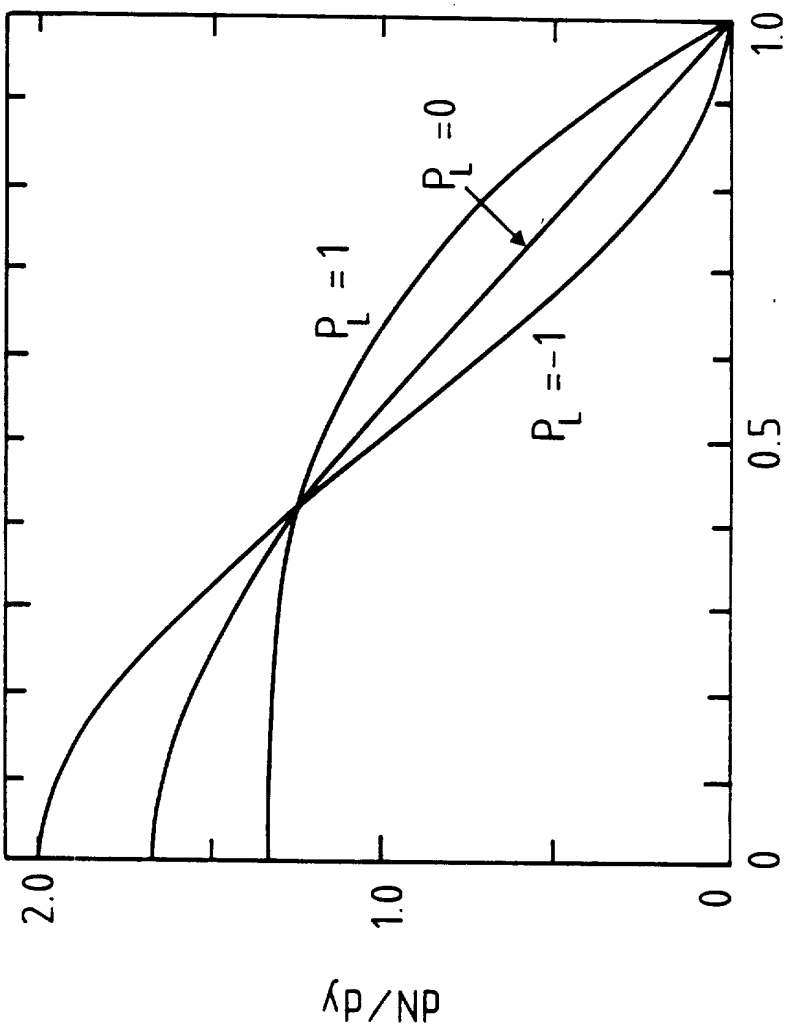

FIG. 4

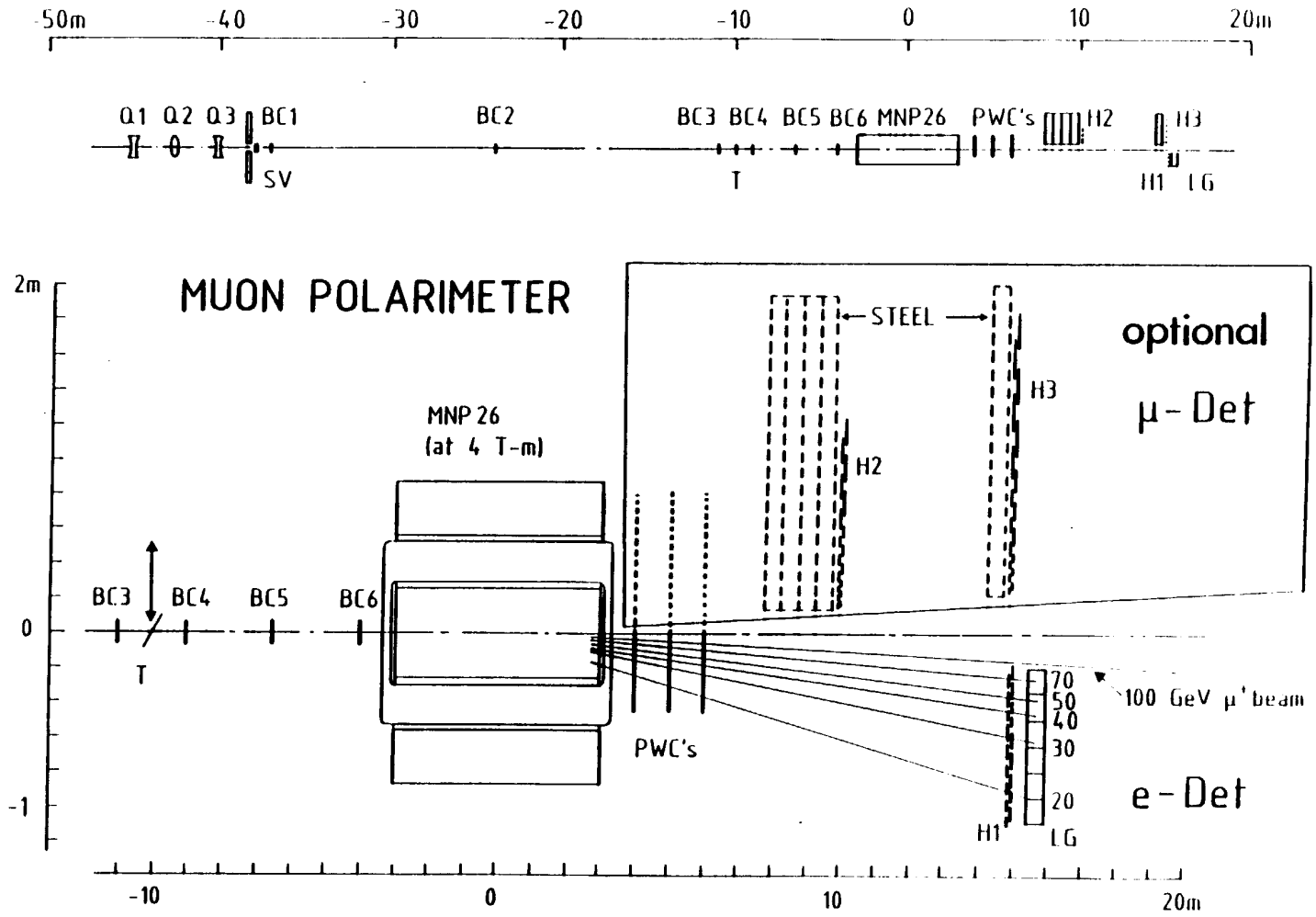
-50m
-40
-30
-20
-10
0
10
20m
Q1 Q2 Q3 BC1
BC2
BC3 BC4 BC5 BC6 MNP26
PWC's
H2
H3
SV
T
H1 LG
MUON POLARIMETER
2m
0
-1
STEEL
optional
μ-Det
H3
MNP 26
(at 4 T-m)
H2
BC3
BC4
BC5
BC6
T
PWC's
70
50
40
30
20
100 GeV μ' beam
e-Det
H1
LG
-10
0
10
20m

FIG. 5

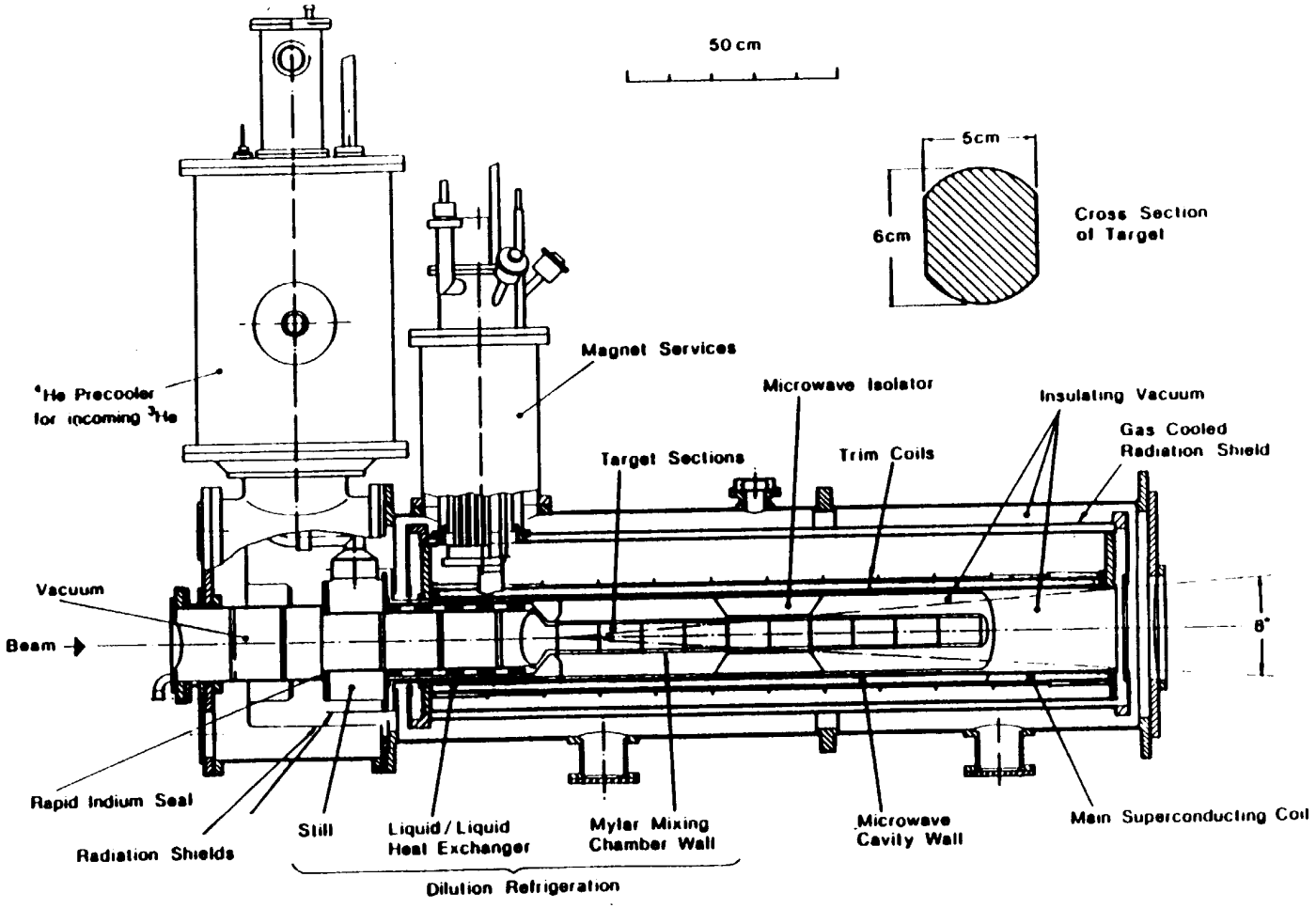
50 cm
5cm
6cm
Cross Section of Target
Magnet Services
⁴He Precooler for incoming ³He
Microwave Isolator
Insulating Vacuum
Gas Cooled Radiation Shield
Target Sections
Trim Coils
Vacuum
Beam
8"
Rapid Indium Seal
Radiation Shields
Still
Liquid / Liquid Heat Exchanger
Mylar Mixing Chamber Wall
Microwave Cavity Wall
Main Superconducting Coil
Dilution Refrigeration

FIG. 6

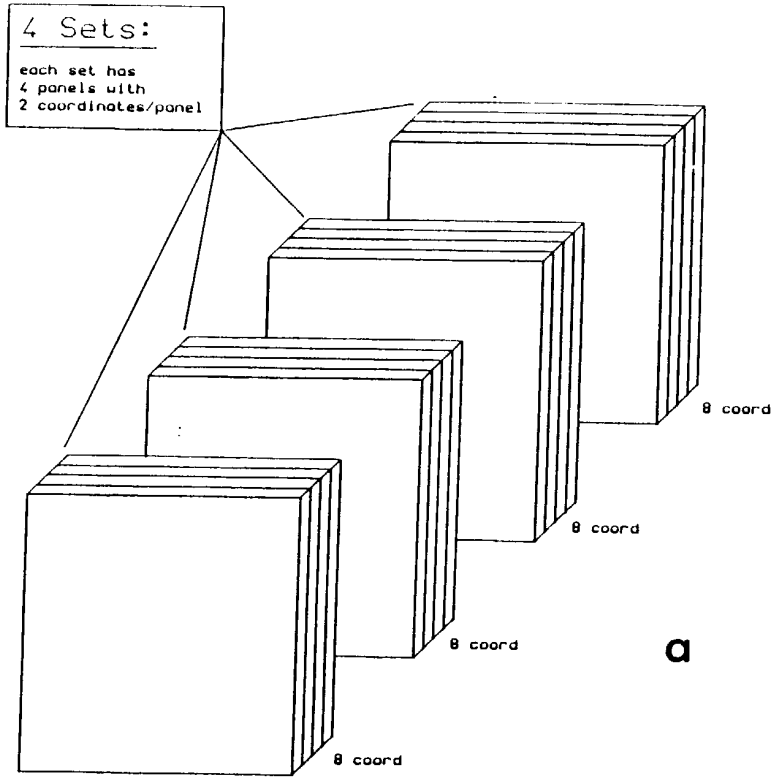

32 coordinates total

new muon chambers W67 built from streamer tubes

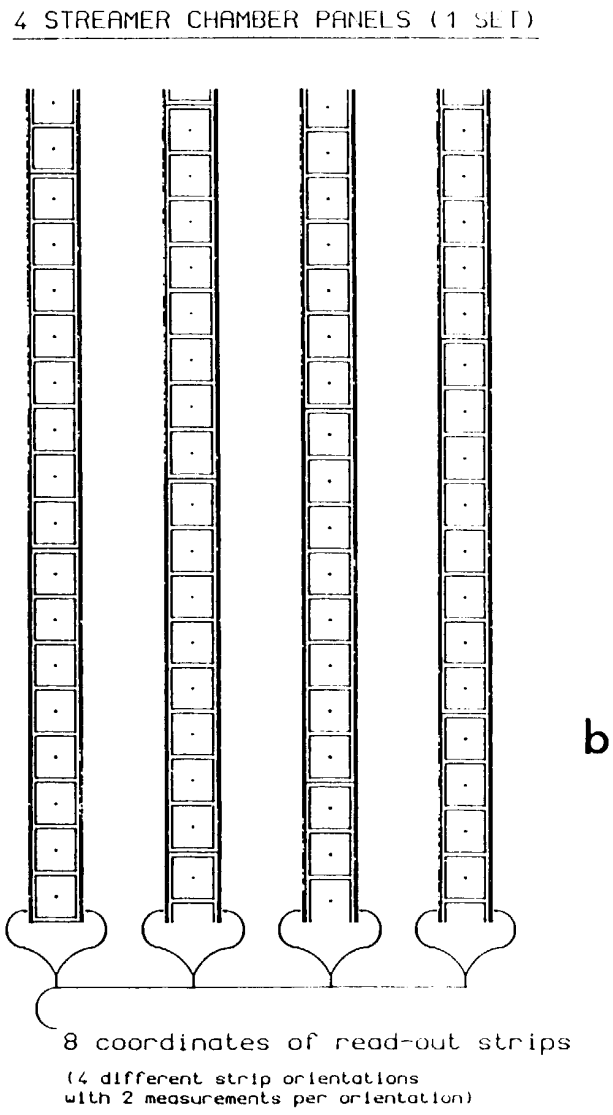

FIG. 7

APPENDIX 1

A MEASUREMENT OF THE SPIN ASYMMETRY AND DETERMINATION OF THE STRUCTURE FUNCTION g_1 IN DEEP INELASTIC MUON-PROTON SCATTERING

European Muon Collaboration

Aachen, CERN, Freiburg, Heidelberg, Lancaster, LAPP (Annecy), Liverpool, Marseille, Mons, Oxford, Rutherford, Sheffield, Turin, Uppsala, Warsaw, Wuppertal, Yale

J. ASHMAN [a], B. BADELEK [b,1], G. BAUM [c,2], J. BEAUFAYS [d], C.P. BEE [e], C. BENCHOUK [f], I.G. BIRD [g,3], S.C. BROWN [e,4], M.C. CAPUTO [c], H.W.K. CHEUNG [h], J. CHIMA [i,5], J. CIBOROWSKI [b,1], R.W. CLIFFT [i], G. COIGNET [j], F. COMBLEY [k], G. COURT [e], G. D'AGOSTINI [f], J. DREES [k], M. DÜREN [g], N. DYCE [g], A.W. EDWARDS [k,6], M. EDWARDS [i], T. ERNST [m], M.I. FERRERO [n], D. FRANCIS [e], E. GABATHULER [e], J. GAJEWSKI [b,1], R. GAMET [e], V. GIBSON [h,7], J. GILLIES [h], P. GRAFSTRÖM [o,7], K. HAMACHER [k], D. VON HARRACH [p], P. HAYMAN [e], J.R. HOLT [e], V.W. HUGHES [c], A. JACHOLKOWSKA [d,8], T. JONES [e,9], E.M. KABUSS [m,3], B. KORZEN [k], U. KRÜNER [k], S. KULLANDER [o], U. LANDGRAF [m], D. LANSKE [g], F. LETTENSTRÖM [o], T. LINDQVIST [o], J. LOKEN [h], M. MATTHEWS [e], Y. MIZUNO [p], K. MÖNIG [k], F. MONTANET [f,7], J. NASSALSKI [b,10], T. NIINIKOSKI [d], P.R. NORTON [i], G. OAKHAM [i,11], R.F. OPPENHEIM [c,12], A.M. OSBORNE [d], V. PAPAVASSILIOU [c], N. PAVEL [k], C. PERONI [n], H. PESCHEL [k], R. PIEGAIA [c], B. PIETRZYK [f], U. PIETRZYK [k,13], B. POVH [p], P. RENTON [h], J.M. RIEUBLAND [d], A. RIJLLART [d], K. RITH [m,3], E. RONDIO [b,1], L. ROPELEWSKI [b,1], D. SALMON [o,9], A. SANDACZ [b,10], T. SCHRÖDER [m], K.P. SCHÜLER [c], K. SCHULTZE [g], T.-A. SHIBATA [p], T. SLOAN [g], A. STAIANO [n,14], H. STIER [m], J. STOCK [m], G.N. TAYLOR [h,15], J.C. THOMPSON [i], T. WALCHER [n,16], S. WHEELER [o,7], W.S.C. WILLIAMS [h], S.J. WIMPENNY [e,17], R. WINDMOLDERS [q], W.J. WOMERSLEY [h,18] and K. ZIEMONS [k]

[a] *Department of Physics, University of Sheffield, Sheffield S3 7RH, UK*
[b] *Physics Institute, University of Warsaw, PL-00681 Warsaw, Poland and Institute for Nuclear Studies, PL-00681 Warsaw, Poland*
[c] *Physics Department, Yale University, New Haven, CT 06520, USA*
[d] *CERN, CH-1211 Geneva 23, Switzerland*
[e] *Department of Physics, University of Liverpool, Liverpool L69 3BX, UK*
[f] *Centre de Physique des Particules, Faculté des Sciences de Luminy, F-13288 Marseille, France*
[g] *Department of Physics, University of Lancaster, Lancaster LA1 4YB, UK*
[h] *Nuclear Laboratory, University of Oxford, Oxford OX1 3RH, UK*
[i] *Rutherford-Appleton Laboratory, Chilton, Didcot, Oxon OX11 0QX, UK*
[j] *Laboratoire de Physique des Particules, IN2P3, F-74019 Annecy-le-Vieux, France*
[k] *Fachbereich Physik, Universität Wuppertal, D-5600 Wuppertal, Fed. Rep. Germany*
[l] *III. Physikalisches Institut A, Physikzentrum, D-5100 Aachen, Fed. Rep. Germany*
[m] *Fakultät für Physik, Universität Freiburg, D-7800 Freiburg, Fed. Rep. Germany*
[n] *Istituto di Fisica, Università di Torino, I-10125 Turin, Italy*
[o] *Gustav Werners Institut, University of Uppsala, S-75121 Uppsala, Sweden*
[p] *Max-Planck Institut für Kernphysik, D-6900 Heidelberg, Fed. Rep. Germany*
[q] *Faculté des Sciences, Université de L'Etat à Mons, B-7000 Mons, Belgium*

Received 22 December 1987; revised manuscript received 5 March 1988

For footnotes see next page.

0370-2693/88/$ 03.50 © Elsevier Science Publishers B.V.
(North-Holland Physics Publishing Division)

The spin asymmetry in deep inelastic scattering of longitudinally polarised muons by longitudinally polarised protons has been measured over a large x range ($0.01 < x < 0.7$). The spin-dependent structure function $g_1(x)$ for the proton has been determined and its integral over x found to be $0.114 \pm 0.012 \pm 0.026$, in disagreement with the Ellis–Jaffe sum rule. Assuming the validity of the Bjorken sum rule, this result implies a significant negative value for the integral of g_1 for the neutron. These values for the integrals of g_1 lead to the conclusion that the total quark spin constitutes a rather small fraction of the spin of the nucleon.

Deep inelastic scattering of polarised charged leptons from polarised targets provides a method of studying the internal spin structure of the nucleon [1–6]. The important quantity obtained from the measurements is the virtual photon–nucleon spin dependent asymmetry A_1 from which the spin-dependent nucleon structure function g_1 can be derived. The asymmetry A_1 is $(\sigma_{1/2}-\sigma_{3/2})/(\sigma_{1/2}+\sigma_{3/2})$ where $\sigma_{1/2}$ ($\sigma_{3/2}$) is the photoabsorption cross section when the projection of the total angular momentum of the virtual photon–nucleon system along the virtual photon direction is 1/2 (3/2). In the quark–parton model the structure function $g_1(x)$ is related to the difference of the quark distributions for quarks with helicities parallel and antiparallel to the nucleon spin.

The measured asymmetry (A) from scattering longitudinally polarised leptons by longitudinally polarised nucleons is defined as

$$A = \frac{d\sigma^{\rightarrow\leftarrow} - d\sigma^{\rightarrow\rightarrow}}{d\sigma^{\rightarrow\leftarrow} + d\sigma^{\rightarrow\rightarrow}}, \qquad (1)$$

where $d\sigma^{\rightarrow\rightarrow(\leftarrow)}$ is the cross section when the lepton and nucleon spins are parallel (antiparallel). In the single-photon exchange approximation, A is related to the virtual photon–nucleon asymmetries A_1 and $A_2 = \sigma_{TL}/\sigma_T$ by

$$A = D(A_1 + \eta A_2), \qquad (2)$$

Here $\sigma_T = \frac{1}{2}(\sigma_{1/2}+\sigma_{3/2})$ is the total transverse cross section and σ_{TL} is the contribution to the cross section resulting from the interference of the transverse and longitudinal amplitudes. D is the depolarisation factor of the virtual photon given by $y(2-y)/[y^2+2(1-y)(1+R)]$ and η is $2(1-y)\sqrt{Q^2}/[Ey(2-y)]$. The standard kinematic variables of deep inelastic scattering are used in these formulae. The incident lepton energy is E; ν and $-Q^2$ are the energy transfer in the laboratory frame and the four-momentum transfer, respectively, and $y = \nu/E$. $R = \sigma_L/\sigma_T$ is the ratio of the longitudinal to transverse virtual photoabsorption cross sections and is small in the energy range of this experiment [7]. See refs. [5,8] for a review of the notation. The asymmetries A_1 and A_2 are bounded by positivity limits to be $|A_1| \leq 1$ and $|A_2| \leq \sqrt{R}$ [9]. Since both R and η are small in the kinematic range of the experiment, A_1 is the dominant contribution to the measured asymmetry A.

The asymmetries A_1 and A_2 are related to the spin-dependent nucleon structure functions $g_1(x, Q^2)$ and $g_2(x, Q^2)$ by

$$A_1 = \frac{2x(1+R)}{F_2}[g_1 - (2Mx/Ey)g_2],$$

$$A_2 = \frac{2x(1+R)}{F_2}(2Mx/Ey)^{1/2}(g_1+g_2), \qquad (3)$$

where M is the nucleon mass, $x = Q^2/2M\nu$ and F_2 is the spin averaged nucleon structure function (the explicit (x, Q^2) dependence of the structure functions

[1] University of Warsaw, PL-00681 Warsaw, Poland, partly supported by CPBP-01.06.
[2] Permanent address, University of Bielefeld, D-4800 Bielefeld, Fed. Rep. Germany.
[3] Present address: MPI für Kernphysik, D-6900 Heidelberg, Fed. Rep. Germany.
[4] Present address: TESA S.A., Renens, Switzerland.
[5] Present address: British Telecom, Ipswich, UK.
[6] Present address: Jet, Joint Undertaking, Abingdon, UK.
[7] Present address: CERN, CH-1211 Geneva 23, Switzerland.
[8] Present address: LAL, F-91405 Orsay, France.
[9] Present address: RAL, Chilton, Didcot, Oxon OX11 0QX, UK.
[10] Institute for Nuclear Studies, PL-00681 Warsaw, Poland, partly supported by CPBP-01.09.
[11] Present address: NRC, Ottawa, Ontario, Canada K1A 0R6.
[12] Present address: AT&T, Bell Laboratories, Naperville, IL, USA.
[13] Present address: MPI für Neurologische Forschung, D-5000 Cologne, Fed. Rep. Germany.
[14] Present address: INFN, I-10125 Turin, Italy.
[15] Present address: University of Melbourne, Parkville, Victoria 3052, Australia.
[16] Present address: University of Mainz, D-6500 Mainz, Fed. Rep. Germany.
[17] Present address: University of California, Riverside, CA 92521, USA.
[18] Present address: University of Florida, Gainesville, FL 32611, USA.

has been omitted, for brevity). Hence g_1 is given by

$$g_1 = \frac{F_2}{2x(1+R)}\,[A_1 + (2mx/Ey)^{1/2}A_2]$$

$$\simeq \frac{F_2 A_1}{2x(1+R)}\,. \qquad (4)$$

In the quark-parton model (in the scaling limit) g_1 is given by [2,10]

$$g_1(x) = \tfrac{1}{2}\sum e_i^2\,[q_i^+(x) - q_i^-(x)]\,, \qquad (5)$$

where e_i is the charge of the quark flavour i and $q_i^{+(-)}(x)$ is the distribution function for a quark of momentum fraction x having the same (+) or opposite (−) helicity to that of the nucleon.

The Bjorken sum rule [1,11] relates the integral of $g_1(x)$ to the ratio of the axial and vector coupling constants G_A and G_V measured in nucleon β decay. After correction for QCD radiative effects [12], this fundamental sum rule is given by

$$\int_0^1 \mathrm{d}x\,[g_1^p(x) - g_1^n(x)] = \tfrac{1}{6}\,|G_A/G_V|\,(1-\alpha_s/\pi)$$

$$= 0.191 \pm 0.002 \quad \text{for } \alpha_s = 0.27 \pm 0.02\,. \qquad (6)$$

Separate sum rules for the proton and neutron have been derived by Ellis and Jaffe [13] using SU(3) current algebra with the assumption of an unpolarised strange quark sea. These sum rules are given by

$$\int_0^1 g_1^{p(n)}(x)\,\mathrm{d}x$$

$$= \frac{1}{12}\left|\frac{G_A}{G_V}\right|\left(+(-)1 + \frac{5}{3}\,\frac{3F/D-1}{F/D+1}\right). \qquad (7)$$

Again after correcting for QCD radiative effects [14] the integrals have values 0.189 ± 0.005 and -0.002 ± 0.005 for the proton and neutron respectively, using the current values of the ratio of the SU(3) couplings $F/D = 0.632 \pm 0.024$ [15] and the value $G_A/G_V = 1.254 \pm 0.006$. Because of the x in the denominator of eq. (4), the small x region is expected to make a large contribution to the integrals.

This paper reports the results of an experiment in which A_1 was measured using high energy polarised muons and a polarised proton target, where the range of x extended from 0.01 to 0.7 and that of Q^2 from 1.5 to 70 GeV^2. The experiment was performed in the M2 muon beam of the CERN SPS accelerator. The muon beam polarisation can be chosen by selecting a specific ratio of the parent pion to decay muon momenta. The polarisation was calculated using a Monte Carlo simulation [16] to be $(82 \pm 6)\%$ at 200 GeV where the error comes mainly from the uncertainty in the pion beam phase space. This calculation is in good agreement with a previous measurement [17] of the polarisation of the same beam.

Data were collected in eleven separate experimental running periods at beam energies of 100, 120 and 200 GeV. Scattered muons and forward produced charged hadrons were detected and measured in the EMC forward spectrometer [18], modified [19] to run at the higher beam intensities necessary for this experiment.

The polarised target has been described in detail elsewhere [20]. The target consisted of two sections, each of a length 360 mm, which were polarised simultaneously in opposite directions. The two sections were separated by a gap of length 220 mm, chosen such that reconstructed vertices from each section could be clearly separated. The target material was irradiated ammonia, chosen because of its relatively high free proton content and its resistance to radiation damage. Peak proton polarisations of more than 80% were obtained with typical values in the range 75–80%, measured with an accuracy ± 5%.

The asymmetry A is obtained from the measured asymmetry Δ by

$$\Delta = \frac{N_1 - N_2}{N_1 + N_2} = P_T P_B f A\,, \qquad (8)$$

where N_1, N_2 are the numbers of events from the two target halves, P_T, P_B are the target and beam polarisations, respectively, and f is the fraction of the events originating from the polarised free protons in the target. Here, f is a function of x since it depends on the neutron-to-proton cross section ratio. The value of Δ is less than 2% over most of the kinematic range of the experiment, requiring strict control of systematic effects to measure it. This was the reason for having a split target which ensured identical beam fluxes and apparatus conditions for both orientations of polarisation.

To compensate for the slightly differing geometric acceptances of the two target halves, the polarisation

directions were reversed during each data taking period, and the values of A obtained for each configuration were averaged. Hence the only systematic effects remaining were due to possible changes in the ratio of the acceptances of the two target halves before and after polarisation reversal. These effects were studied by splitting the data in different ways into two samples, one of which was expected to suffer much more acceptance changes. The consistency of the results obtained from the two samples showed no indication of residual systematic effects beyond the statistical errors.

The cuts applied to the data were similar to those used in previous EMC analyses [7]. The muon scattering angle cut was increased to 1° to ensure good resolution of events coming from the two target halves. A total of 1.2×10^6 events survived these cuts.

Corrections to the dilution factor f were applied for the smearing of events into the target halves which originated in the unpolarised material around the target ($\sim6\%$) and kinematic smearing due to the intrinsic resolution of the track measurements ($<3\%$), using a Monte Carlo simulation of the experiment. Corrections ($\sim1.5\%$) were also applied for the slight polarisation of the nitrogen nucleus [21], and for higher order radiative effects [22,23] (2–20%). The contribution to the asymmetry from electroweak interference was calculated and found to be negligible.

The values of A_1 are given in table 1, where ηA_2 has been neglected so that $A_1 \simeq A/D$. These values were obtained by statistically combining the results from the 11 data taking periods. The consistency of the various periods is shown by the χ^2 to the mean value, given in table 1. These values of χ^2 follow a reasonable statistical distribution, showing that time dependent systematic effects were well controlled. The systematic errors given in table 1 include the uncertainties in the value of R (50% of its value) which was taken to be the value calculated from QCD [24,25], the uncertainty in neglecting A_2 in eqs. (2) and (4) (taking $A_2 = \pm\sqrt{R}$), the uncertainty in f arising from the error in the measured neutron-to-proton cross section ratio and nuclear effects on the structure function F_2 in nitrogen, and the error due to radiative corrections. They also include an estimate of the possible systematic error, as described above, arising from time dependent acceptance changes.

The results for A_1^p are plotted in fig. 1 together with those of previous SLAC experiments [26,27], which are in good agreement with our results in the region of overlap. The prediction of the model of Carlitz and Kaur [28] is also shown. This model gives a good representation of the data at large x but fails to reproduce it for $x<0.2$. In fig. 2 values of A_1^p in several x are plotted versus Q^2 to search for scaling violations. These are expected to be small [6,29], and we conclude that within errors the data are consistent with scaling. This justifies combining the data from periods with different beam energies. A good fit to the data in fig. 1 is given by

$$A_1^p(x) = 1.04x^{0.16}[1-\exp(-2.9x)]\,.$$

The spin-dependent structure function $g_1^p(x)$ was obtained from $A_1^p(x)$ using eq. (4), setting R to the value calculated from QCD. The values of F_1^p were

Table 1
Results for A_1 in x bins. There is a further 9.6% normalisation error on A_1 due to uncertainties in the beam and target polarisations.

x range	$\langle x\rangle$	$\langle Q^2\rangle$ $(\mathrm{GeV}/c)^2$	$A_1 \pm$ stat. $\pm$ syst.	χ^2/DOF
0.01–0.02	0.015	3.5	$0.021\pm0.035\pm0.017$	6.8/10
0.02–0.03	0.025	4.5	$0.087\pm0.043\pm0.022$	9.7/10
0.03–0.04	0.035	6.0	$0.013\pm0.054\pm0.024$	5.3/10
0.04–0.06	0.050	8.0	$0.094\pm0.048\pm0.028$	4.0/10
0.06–0.10	0.078	10.3	$0.139\pm0.049\pm0.037$	4.3/10
0.10–0.15	0.124	12.9	$0.169\pm0.063\pm0.045$	19.8/10
0.15–0.20	0.175	15.2	$0.360\pm0.087\pm0.057$	14.9/10
0.20–0.30	0.248	18.0	$0.469\pm0.088\pm0.065$	13.3/10
0.30–0.40	0.344	22.5	$0.517\pm0.141\pm0.068$	9.8/10
0.40–0.70	0.466	29.5	$0.657\pm0.175\pm0.065$	8.4/10

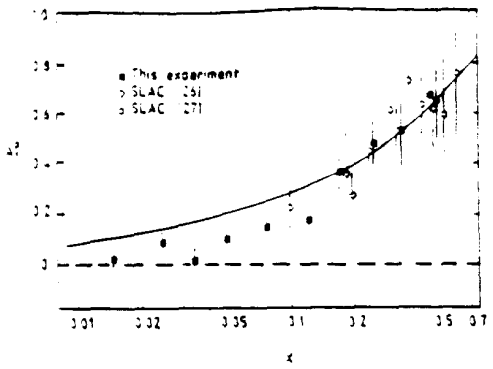

Fig. 1. The asymmetry A_1^p plotted versus x together with results from previous experiments [26,27]. The curve is from the model of ref. [28].

taken from ref. [7] but corrected from the value $R=0$ assumed in that paper to the QCD value of R. Fig. 3 shows $xg_1^p(x)$ as a function of x. The solid curve is

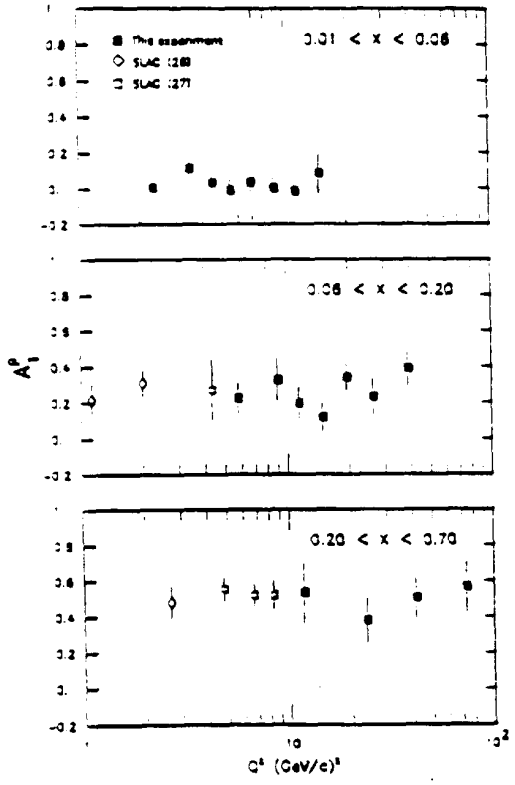

Fig. 2. A_1^p versus Q^2. The data in each x range have been corrected to the same mean x using a fit to the data as a function of x.

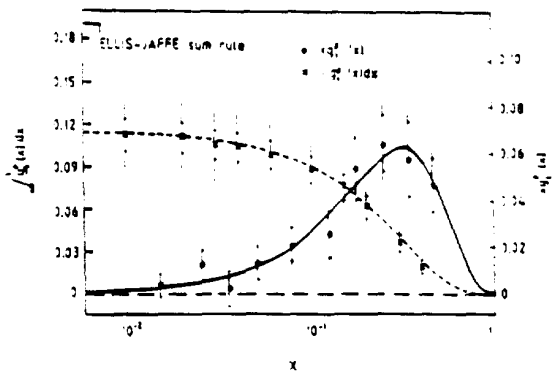

Fig. 3. The quantity $xg_1^p(x)$ (right-hand axis and solid circles) versus x. The left-hand axis and the crosses show the values of $\int_{x_m}^1 g_1^p(x)dx$ where x_m is the value of x at each lower bin edge. The inner error bars are statistical and the outer error bars are the total errors obtained by combining the statistical and systematic errors (table 1) in quadrature. The curves are described in the text.

derived from the fitted function to $A_1^p(x)$. The integral of $g_1^p(x)$ over the measured region was found to be

$$\int_{0.01}^{0.7} g_1^p(x)dx = 0.111 \pm 0.012(\text{stat.}) \pm 0.026\ (\text{syst.})\ .$$

The convergence of this integral is also shown in fig. 3 where $\int_{x_m}^1 g_1^p(x)dx$ is plotted as a function of x_m, the value of x at the lower edge of each bin. It can be seen that the integral converges well towards $x=0$. The dashed curve is the integral of the solid curve and this was used to extrapolate to $x=0$. The data covered 98% of the value of the integral. The value obtained at a mean Q^2 of 10.7 GeV^2 was

$$\int_0^1 g_1^p(x)dx = 0.114 \pm 0.012(\text{stat.}) \pm 0.026(\text{syst.})\ .$$

Here the systematic error was obtained from the individual systematic errors, added in quadrature and includes a further uncertainty of 10% on the value of the integral to allow for possible errors on the value of F_2 for the proton. The uncertainty due to the extrapolation outside the measured range of x is small providing that $xg_1(x)$ is well behaved and approaches zero reasonably as x tends to zero. It is expected from Regge theory [30] that $xg_1(x)$

approaches zero linearly with x at small x and such behaviour is compatible with the data in the range $0.01 < x < 0.1$. If, however, $xg_1(x)$ approaches zero as $(1/\ln x)^2$ as predicted by an alternative Regge model [30] the value of the integral increases by 0.018 which is within the quoted systematic error. Such behaviour would imply that $g_1(x)$ diverges as x approaches zero i.e. the quarks remain strongly polarised, which seems unreasonable. This also applies to any other functional form for $xg_1(x)$ which tends to zero more slowly than linearly with x.

Our value for the integral of $g_1^p(x)$ is compatible with the previously measured value of 0.17 ± 0.05 [27] where the uncertainty is dominated by the extrapolation to low x. However, it is smaller than the value 0.189 ± 0.005 expected from the Ellis–Jaffe sum rule. It is also smaller than the value 0.17 ± 0.03 derived from a calculation based on QCD sum rule methods [31] and that (0.205) expected from the model [28] of the spin structure of the nucleon. As we show later, the discrepancy with the Ellis–Jaffe sum rule could be due to a polarisation of the strange sea antiparallel to that of the proton, although a perturbative QCD calculation for the generation of the sea [32] does not predict such an effect. Another possible explanation has recently been offered by Jaffe [33] in view of the non-conservation of the U(1) axial current in QCD, a consequence of the Adler–Bell–Jackiw anomaly [34,35]. Although the precise size of the effect is currently uncalculable, Jaffe gives a lower limit for the proton sum rule of 0.113 which is compatible with the measurement presented here.

The integral of $g_1^n(x)$ was expected to be close to zero according to the Ellis–Jaffe sum rule. Using our value for the integral of $g_1^p(x)$, and assuming the validity of the Bjorken sum rule, we obtain a value of $-0.077 \pm 0.012(\text{stat.}) \pm 0.026(\text{syst.})$ for the integral of $g_1^n(x)$. Hence polarised lepton–neutron scattering should show a significant negative asymmetry over at least part of the x range.

Using the above values for the integrals of $g_1^{p(n)}(x)$, the net spin carried by the quarks in the nucleon can be deduced. Integrating the quark–parton model expression for $g_1(x)$ (eq. (5)) and including first order QCD correlations, we obtain

$$2\int_0^1 g_1^p(x)\,dx = \tfrac{1}{9}\Delta u[1-(\alpha_s/2\pi)(C_f+1)] + \tfrac{1}{9}\Delta d[1-(\alpha_s/\pi)(2C_f-1)] + \tfrac{1}{9}\Delta s[1-(\alpha_s/\pi)(2C_f-1)],$$

where $C_f = (33-8f)/(33-2f)$ with f the number of quark flavours and

$$\Delta u = \int_0^1 [q_u^+(x) + q_{\bar{u}}^+(x) - q_u^-(x) - q_{\bar{u}}^-(x)]\,dx,$$

etc. The corresponding expression for $g_1^n(x)$ is obtained by interchanging Δu and Δd. If we assume an unpolarised strange quark sea ($\Delta s = 0$) these expressions become

$$2\int_0^1 g_1^p(x)\,dx = \frac{3.82}{9}\Delta u + \frac{1.08}{9}\Delta d = 0.228 \pm 0.024 \pm 0.052,$$

$$2\int_0^1 g_1^n(x)\,dx = \frac{1.08}{9}\Delta u + \frac{3.82}{9}\Delta d = -0.154 \pm 0.024 \pm 0.052.$$

Hence the mean z component of the spin, S_z, of the u flavoured quarks in a proton with $S_z = +\frac{1}{2}$ is

$$\langle S_z\rangle_u = \tfrac{1}{2}\Delta u = 0.348 \pm 0.023 \pm 0.051,$$

and that of the d flavoured quarks is

$$\langle S_z\rangle_d = \tfrac{1}{2}\Delta d = -0.280 \pm 0.023 \pm 0.051.$$

Thus the mean S_z of the quarks is

$$\langle S_z\rangle_{u+d} = 0.068 \pm 0.047 \pm 0.103.$$

Hence $(14 \pm 9 \pm 21)\%$ of the proton spin is carried by the spin of the quarks. The remaining spin must be carried by gluons or orbital angular momentum [36,37].

If we assume the discrepancy between our result and the Ellis–Jaffe sum rule prediction to be due to the polarisation of the strange quark sea we obtain

$$\langle S_z\rangle_u = 0.373 \pm 0.019 \pm 0.039,$$

$$\langle S_z\rangle_d = -0.254 \pm 0.019 \pm 0.039,$$

$$\langle S_z\rangle_s = -0.113 \pm 0.019 \pm 0.039,$$

$$\langle S_z\rangle_{u+d+s} = 0.006 \pm 0.058 \pm 0.117,$$

indicating that the quark spins carry $(1 \pm 12 \pm 24)\%$ of the proton spin.

In conclusion, measurements have been presented of the spin asymmetries in deep inelastic scattering of polarised muons on polarised protons. The spin-dependent structure function g_1 of the proton has also been determined. The integral $\int_0^1 g_1^p(x)\mathrm{d}x = 0.114 \pm 0.012 \pm 0.026$ is significantly lower than the value expected from the Ellis–Jaffe sum rule. Assuming the validity of the Bjorken sum rule this result implies that the asymmetry measured from polarised neutrons should be significantly negative over at least part of its x range. In addition, the result implies that, in the scaling limit, a rather small fraction of the spin of the proton is carried by the spin of the quarks.

References

[1] J.D. Bjorken, Phys. Rev. 148 (1966) 1467.
[2] J. Kuti and V.F. Weisskopf, Phys. Rev. D 4 (1971) 3418.
[3] A.J.G. Hey and J.E. Mandula, Phys. Rev. D 5 (1972) 2610.
[4] N.S. Craigie et al., Phys. Rep. 99 (1983) 69.
[5] V.W. Hughes and J. Kuti, Annu. Rev. Nucl. Part. Sci. 33 (1983) 611.
[6] E. Gabathuler, Proc. 6th Intern. Symp. on High energy spin physics (Marseille, 1984), ed. J. Soffer.
[7] F. Sciulli, Proc. Intern. Symp. on Lepton and photon interactions at high energies (Kyoto, 1985), eds. M. Konuma and K. Takahashi.
[8] EM Collab., J.J. Aubert et al., Nucl. Phys. B 259 (1985) 189.
[9] M.G. Doncel and E. de Rafael, Nuovo Cimento 4 A (1971) 363.
[10] R.P. Feynman, Photon–hadron interactions (Benjamin, New York, 1972).
[11] J.D. Bjorken, Phys. Rev. D 1 (1970) 1376.
[12] J. Kodaira et al., Phys. Rev. D 20 (1979) 627; Nucl. Phys. B 159 (1979) 99.
[13] J. Ellis and R.L. Jaffe, Phys. Rev. D 9 (1974) 1444; D 10 (1974) 1669(E).
[14] J. Kodaira, Nucl. Phys. B 165 (1980) 129.
[15] M. Bourquin et al., Z. Phys. C 21 (1983) 27.
[16] C. Iselin, A computer programme to calculate muon halo, CERN report CERN 74-17 (1974).
[17] D. Bollini et al., Nuovo Cimento 63 A (1981) 441.
[18] EM Collab., O.C. Allkofer et al., Nucl. Instrum. Methods 179 (1981) 445.
[19] EM Collab., J. Ashman et al., to be published.
[20] S.C. Brown et al., Proc. 4th Intern. Workshop on Polarised target materials and techniques (Bonn, 1984), ed. W. Meyer.
[21] G.R. Court and W.G. Heyes, Nucl. Instrum. Methods A 243 (1986) 37.
[22] L.W. Mo and Y.S. Tsai, Rev. Mod. Phys. 41 (1965) 205; Y.S. Tsai, SLAC report SLAC-PUB-848 (1971), unpublished.
[23] T.V. Kukhto and N.M. Shumeiko, Yad. Fiz. 36 (1982) 707.
[24] G. Altarelli and G. Martinelli, Phys. Lett. B 76 (1978) 89.
[25] M. Glück and E. Reya, Nucl. Phys. B 145 (1978) 24.
[26] M.J. Alguard et al., Phys. Rev. Lett. 37 (1976) 1261; 41 (1978) 70.
[27] G. Baum et al., Phys. Rev. Lett. 51 (1983) 1135.
[28] R. Carlitz and J. Kaur, Phys. Rev. Lett. 38 (1977) 673; J. Kaur, Nucl. Phys. B 128 (1977) 219.
[29] O. Darrigol and F. Hayot, Nucl. Phys. B 141 (1978) 391.
[30] B.L. Ioffe, V.A. Khoze and L.N. Lipatof, Hard processes (North-Holland, Amsterdam, 1984) p. 61.
[31] V.M. Belyaev, B.L. Ioffe and Y.I. Kogan, Phys. Lett. B 151 (1985) 290.
[32] F.E. Close and D. Sivers, Phys. Rev. Lett. 39 (1977) 1116.
[33] R.L. Jaffe, Phys. Lett. B 193 (1987) 101.
[34] S.L. Adler, Phys. Rev. 177 (1969) 2426.
[35] J.S. Bell and R. Jackiw, Nuovo Cimento 60 A (1969) 47.
[36] L.M. Sehgal, Phys. Rev. D 10 (1974) 1663.
[37] P.G. Ratcliffe, Phys. Lett. B 192 (1987) 180.

APPENDIX 2

THE INTEGRAL OF THE SPIN-DEPENDENT STRUCTURE FUNCTION g_1^p AND THE ELLIS–JAFFE SUM RULE

V.W. HUGHES, V. PAPAVASSILIOU, R. PIEGAIA, K.P. SCHÜLER
Yale University, New Haven, CT 06520, USA

and

G. BAUM
University of Bielefeld, D-4800 Bielefeld, Fed. Rep. Germany

Received 15 July 1988

A recent EMC experiment has found that the integral of the spin-dependent structure function g_1 of the proton violates the Ellis–Jaffe sum rule. It is shown here that this result can be strengthened when combined with older data from SLAC.

Recently, an experiment by the European Muon Collaboration (EMC) has measured [1] the asymmetry in deep-inelastic polarized muon–proton scattering at CERN. The asymmetry A_1 is shown in fig. 1 as a function of the Bjorken scaling variable x, together with older data [2,3] from polarized electron–proton scattering at lower beam energies at SLAC. The agreement of the CERN and SLAC data is very good. From A_1, the spin-dependent structure function g_1 of the proton was computed, using the relation

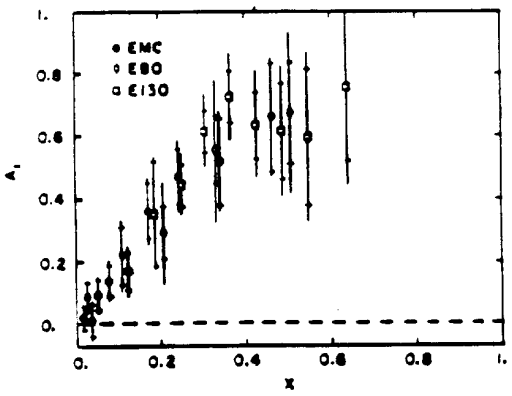

Fig. 1. Compilation of all the data on A_1^p as a function of x. The EMC points (ref. [1]) are shown as full circles while the SLAC points are shown as open diamonds (experiment E-80, ref. [2]) and open squares (E-130, ref. [3]). Inner error bars are the statistical errors and the outer error bars are the total errors (statistical plus systematic added in quadrature). The systematic errors include uncertainties in the values of R and A_2.

$$g_1(x) = \frac{A_1(x)F_2(x)}{2x(1+R)}, \tag{1}$$

where F_2 is the usual spin-independent structure function and R is the ratio of longitudinal and transverse total cross sections. A_1 is related to the measured asymmetry A by $A = D(A_1 + \eta A_2) \simeq DA_1$ where the kinematic factor D also depends on R. The quantity A_2 is a second asymmetry and η is a small kinematic factor.

In the EMC experiment the integral of g_1 over x was found to be

$$\int_0^1 g_1^p(x)\mathrm{d}x = 0.114 \pm 0.012 \pm 0.026, \tag{2}$$

where the first error is statistical and the second systematic. This result is in disagreement with the Ellis–Jaffe sum rule [4]. Without the QCD correction this sum rule predicts

0370-2693/88/$ 03.50 © Elsevier Science Publishers B.V.
(North-Holland Physics Publishing Division)

$$\int_0^1 g_1^p(x)\,dx = \frac{1}{12}\,\frac{g_A}{g_V}\left[1+\frac{5}{3}\left(\frac{3\mathcal{F}/\mathcal{D}-1}{\mathcal{F}/\mathcal{D}+1}\right)\right]$$

$$= 0.200 \pm 0.005\,. \qquad (3)$$

Here $g_A/g_V = -1.254 \pm 0.006$ is the ratio of axial-vector and vector weak coupling constants in nucleon β-decay [5]. $\mathcal{F}$ and $\mathcal{D}$ are the SU(3) couplings and the uncertainty in the sum rule is mainly due to the experimental error in the measurement [6] of the ratio $\mathcal{F}/\mathcal{D} = 0.632 \pm 0.024$. The first-order QCD correction [7] reduces the value of the integral in (3) to 0.189 at $Q^2 = 10$ GeV$^2/c^2$. The full circles in fig. 2 show the values for the integral of g_1 from the low edge of each x bin to 1, plotted at the edge of the bin. The solid curve was computed using a fit to the EMC values for A_1. The difference between the theoretical and experimental values is $0.075 \pm 0.012 \pm 0.026$.

The EMC result is consistent with a determination based on the SLAC data, which gave [3]

$$\int_0^1 g_1^p(x)\,dx = 0.17 \pm 0.05\,, \qquad (4)$$

with statistical and systematic errors combined in quadrature. The uncertainty is dominated by the extrapolation to low x (below 0.1) where no data were taken. Due to this large error, the result in (4) is also consistent with the Ellis–Jaffe sum rule.

Since the new and the old data are in agreement over the region of overlap, $0.1 \leq x \leq 0.7$, the total error can be reduced by combining the two results in this region and using the EMC points at low x. For this purpose, it is important to treat the two sets of data in as similar a fashion as possible. Therefore, the SLAC data were re-examined in order to separate the statistical and systematic errors. Point-by-point statistical errors were added in quadrature when computing the integral, while systematic errors were added linearly, to allow for the possibility of common systematic errors affecting all the x bins in the same direction. In addition, uncertainties due to the values of R and A_2, which is unknown except that it is bounded by $|A_2| \leq \sqrt{R}$ were included in the systematic error [*1]. Finally, the data from ref. [2] which were obtained in narrow x bins, were merged into the bins of ref. [3].

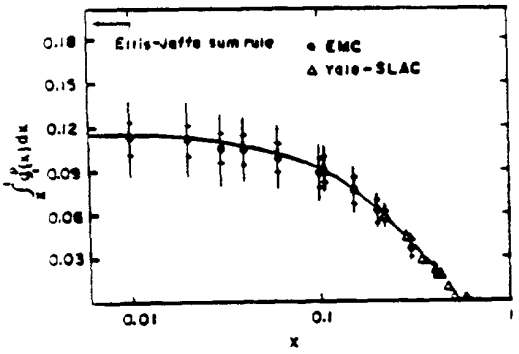

Fig. 2. Results for $\int g_1(x)\,dx$. Full circles: computed from the EMC data [1]. Open triangles: computed from the SLAC data, merging the two experiments [2,3]. The solid curve was computed from a fit to the EMC A_1 data. Inner (outer) error bars are the statistical (total) errors.

The integrals were computed using a parametrization of F_2 taken from ref. [8], at $Q^2 = 10$ GeV$^2/c^2$, the mean Q^2 of the EMC data. Since no evidence for any Q^2 dependence of A_1 was found from the SLAC and EMC data [1–3] it is justified to assume that the A_1 values of the two experiments are valid at this Q^2. For R, a QCD calculation [9] was used. Since $R = 0$ was assumed in extracting F_2 in ref. [8], F_2 was corrected for consistency for the non-zero R values used here (see eq. (2.7) in ref. [8]).

The two data sets give, over the region of overlap,

$$\int_{0.1}^{0.7} g_1^p(x)\,dx = 0.091 \pm 0.008 \pm 0.0013 \quad \text{(SLAC)}\,,$$

$$\int_{0.1}^{0.7} g_1^p(x)\,dx = 0.087 \pm 0.010 \pm 0.015 \quad \text{(EMC)}\,. \qquad (5)$$

The SLAC results for $\int g_1^p dx$ are also shown in fig. 2 (open triangles). The SLAC and EMC results are in excellent agreement.

For the SLAC data, $R = 0.25 \pm 0.10$ was used in computing A_1, as previously done in refs. [2,3]. This number is larger than the QCD prediction [9]. Using the same QCD calculation for the SLAC data, at

[*1] The exact expression for g_1 is $g_1(x) = (F_2(x)/2x(1+R))[A/D + (\sqrt{Q^2}/\nu - \eta)A_2]$. The second term inside the square brackets gives the uncertainty due to the unknown value of A_2. The definition of all the relevant quantities can be found in refs. [1–3].

the appropriate Q^2, would reduce the A_1 values because of the R dependence of D and the first integral in (5) would decrease by 0.012. However, this calculation gives R values that are probably too small for the kinematic range of the SLAC data. A recent experiment at SLAC found [10] that perturbative QCD describes the data on R at these low Q^2 values only if corrections for target-mass effects are included. The parametrization given in ref. [10] implies that R is in the range 0.13–0.29 in the kinematic range of the data of ref. [2] and 0.08–0.16 in that of ref. [3], with the highest R values obtained for the lowest x points (0.10–0.22). With this parametrization of R, the SLAC result above (eq. (5)) is reduced by 0.002.

The systematic errors in the two results above have very different origins, and therefore they can be combined as if they were statistical. This gives

$$\int_{0.1}^{0.7} g_1^p(x)\,dx = 0.089 \pm 0.006 \pm 0.010 . \qquad (6)$$

In addition, EMC alone gives

$$\int_{0.01}^{0.1} g_1^p(x)\,dx = 0.024 \pm 0.007 \pm 0.008 . \qquad (7)$$

In combining (6) and (7), care must be taken regarding the correlation in the uncertainties of the low- and high-x EMC data. If the systematic errors in (6) and (7) were uncorrelated, they should be added in quadrature while if they were correlated they should be added linearly. Since (6) was obtained with approximately equal contributions from SLAC and EMC, the mean of the systematic errors obtained by the two approaches is taken. Adding the contributions of the extrapolations of the EMC data to unmeasured regions $x = 0$–0.01 and $x = 0.7$–1.0 (0.002 and 0.001, respectively), we obtain

$$\int_0^1 g_1^p(x)\,dx = 0.116 \pm 0.009 \pm 0.019 \quad \text{(world average)} , \qquad (8)$$

with the systematic error containing an additional 10% uncertainty arising from the value of F_2 (see ref. [11] for an up-to-date discussion of the experimental situation on F_2).

The combination of the two results makes more pronounced the difference between the experimental and the QCD corrected theoretical values. Combining all errors in quadrature, this difference is

$$\int_0^1 g_1^p(x)\,dx\Big|_{\text{theory}} - \int_0^1 g_1^p(x)\,dx\Big|_{\text{experiment}} = 0.073 \pm 0.022 , \qquad (9)$$

or about 3.5 standard deviations.

One potential explanation for the failure of the sum rule could be that the Q^2 of the experiments is not high enough for asymptotic arguments to apply, therefore the Q^2 evolution of the structure function might conceivably be larger than the one predicted by perturbative QCD. The Drell–Hearn–Gerasimov sum rule [12] for real photoproduction requires that the asymmetry be negative in the limit $Q^2 = 0$ over at least part of the range of the photon energy ν. Hence g_1^p may vary rapidly with Q^2 until its integral reaches the positive value predicted by eq. (3). However the comparison [1] between the low-energy ($\langle Q^2 \rangle \simeq 4\ \text{GeV}^2/c^2$) SLAC data and the higher-energy ($\langle Q^2 \rangle \simeq 10\ \text{GeV}^2/c^2$) EMC data failed to detect any strong Q^2 dependence.

In addition to the data in refs. [2,3], there exist data from SLAC on the asymmetry in the resonance region (missing-mass range $W = 1.1$–1.9 GeV) at even lower Q^2, 0.5 and 1.5 GeV^2/c^2 [13]. The asymmetry is positive practically everywhere except in the region of the $\Delta(1232)$ resonance and is in good agreement with the deep-inelastic data, indicating that the transition from real to virtual photoproduction is essentially complete in the kinematic range of the experiments [1–3]. This is also supported by a partial-wave analysis [14] of unpolarized pion-electroproduction data at $Q^2 = 0.3$–$1.0\ \text{GeV}^2/c^2$.

In conclusion, we have shown that the violation of the Ellis–Jaffe sum rule found by EMC [1] becomes more significant when all the available data [2,3] are included. In addition, the comparison of data taken in different kinematic ranges seems to exclude the possibility that the effect is due to a strong Q^2 dependence.

The authors want to thank the members of the EMC

for many useful discussions. This work was supported in part by the US department of Energy.

References

[1] EM Collab., J. Ashman et al., Phys. Lett. B 206 (1988) 364.
[2] M.J. Alguard et al., Phys. Rev. Lett. 37 (1976) 1261; 41 (1978) 70.
[3] G. Baum et al., Phys. Rev. Lett. 51 (1981) 1135.
[4] J. Ellis and R.L. Jaffe, Phys. Rev. D9 (1974) 1444.
[5] Particle Data Group, M. Aguilar-Benitez et al. Review of particle properties, Phys. Lett. B 170 (1986) 1.
[6] M. Bourquin et al., Z. Phys. C 21 (1983) 27.
[7] J. Kodaira, Nucl. Phys. B 165 (1980) 129.
[8] EM Collab., J.J. Aubert et al., Nucl. Phys. B 259 (1985) 189.
[9] G. Altarelli and G. Martinelli, Phys. Lett. B 76 (1978) 89;
M. Glück and E. Reya, Nucl. Phys. B 145 (1978) 24.
[10] S. Dasu et al., University of Rochester preprint UR-1045 (1988), to be published.
[11] T. Sloan, in: Proc. Intern. Europhysics Conf. on High energy physics, ed. O. Botner (Uppsala, 1987) p. 857;
R. Voss, in: Proc. 13th Intern. Symp. on Lepton and photon interactions at high energies, eds. W. Bartel and R. Rückl (Hamburg, 1988) p. 581.
[12] S.D. Drell and A.C. Hearn, Phys. Rev. Lett. 16 (1966) 908;
S.B. Gerasimov, Sov. J. Nucl. Phys. 2 (1966) 430;
I. Karliner, Phys. Rev. D 7 (1973) 2717.
[13] G. Baum et al., Phys. Rev. Lett. 45 (1980) 2000.
[14] R. Devenish and D. Lyth, Nucl. Phys. B 93 (1975) 109.